THE UNIVERSITY OF CALGARY

FACULTY OF SCIENCE

DEPARTMENT OF GEOLOGY AND GEOPHYSICS

GOPH 703

Arrays

Submitted to: Dr. Edward Krebes
Dr. Don Lawton
Dr. Larry lines

Presented by: Yajaira Herrera
UCID: 989609

Calgary
April 7th, 2005

Introduction

The present project is a compilation of papers published in the area of seismic arrays. “Arrays” is a very broad subject and it is not my intention to cover it fully. Nevertheless, a myriad of issues will be discussed related only to land seismic acquisition.

The report is divided into sections that include each one of the papers studied. A myriad of authors were selected and the quality of their papers vary. Some of them could be classified in the “Classics” category for the legacy given to the seismic industry. On the other hand, there are other papers that one wonders how they got published! Nevertheless, one has to understand the knowledge and techniques available at the time.

Initially, the area of interest for this report was point receivers versus geophone arrays. There is a school of thought that promotes the use of point receivers claiming that they are more beneficial than geophone arrays. Unfortunately, not many papers are published that compare side by side the two methods. Therefore, I decided to widen the scope of the report to field arrays.

Basic aspects of array design are covered at the beginning of the report to set a solid background for the following sections. A case history is presented at the end in which geophone, vibrator disposition and drag arrays are analyzed.

A brief conclusion is presented at the end. The most important conclusion that I reached was that arrays could be very helpful to the seismic data when designed appropriately. It is not only the filtering capabilities they offer, but also the enhancement of the average output and signal-to-noise ratio, as well as the anti-alias properties they provide.

Arrays

Table of Contents

Arrays

List of Figures

Arrays

List of Tables

Arrays

Arrays are filters in the wavenumber domain that attenuate undesired events as noise. They are formed by the physical disposition of geophones and/or sources in the field. They are designed to reject noise past the longest wavenumber of desired signal.

On the surface we measure apparent wavelengths. In **Figure 1** we can see a real waveform as it emerges on the surface and its correspondent apparent wavelength as is registered by the geophones. Given that arrays are wavenumber filters, it is convenient to express wavelengths in the wavenumber domain. The following equations are used assuming a flat reflector:

$$\lambda_{app} = \frac{V}{f \sin\theta} \qquad (1)$$

where λ_{app} is the apparent wavelength, V is the reflector velocity, f is the reflector maximum frequency, and θ is the angle of emergence with respect to the vertical axis and it is represented by:

$$\sin\theta = \frac{X/2}{\sqrt{(X/2)^2 + D^2}} \qquad (2)$$

where X is the source-receiver offset and D is the depth to the reflector.

Wavenumber (k_{app}) is the inverse of the wavelength, so substituting (2) into (1) and solving for k_{app} we get:

$$k_{app} = \frac{f\ X/2}{V\sqrt{(X/2)^2 + D^2}} \qquad (3)$$

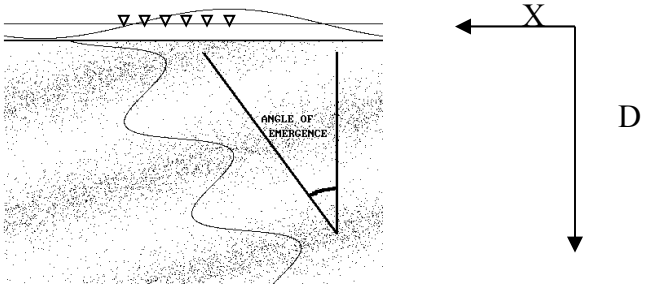

Figure 1
Angle of emergence.
Taken from Cooper, 2000.

When a waveform emerges with a ray path perpendicular to the surface, it has an angle of emergence equal to 0 degrees, as is the case of a reflector with zero dip. The angle of emergence is a function of the offset and depth of the reflector (**Figure 2**), as well as of the dip of the reflector. Shallow, near-offset reflections will produce very long apparent wavelengths represented as the horizontal wave in the left plot, and shallow, far-offset reflections will generate shorter apparent wavelengths as seen in the right plot.

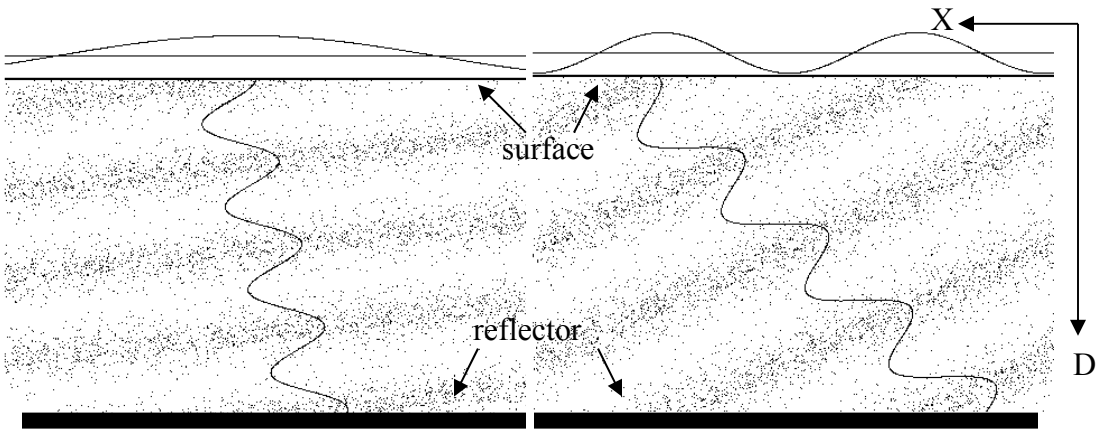

Figure 2
Shallow near offset (left) and far offset (right) wavelengths.
Taken from Cooper, 2000.

In **Table 1** the different apparent wavelengths obtained at the surface are observed. These wavelengths come from a shallow reflector at a depth of 625 m and a velocity of 2500 m/s, as we vary the frequencies from 10 to 90 Hz and the offsets from 100 to 800 m.

V (m/s)	f (s^{-1})	X (m)	D (m)	θ	k_{app} (m^{-1})	λ_{app} (m)
2500	10	100	625	4.57	0.0003	3135
2500	10	800	625	32.62	0.0022	464
2500	30	100	625	4.57	0.0010	1045
2500	30	800	625	32.62	0.0065	155
2500	60	100	625	4.57	0.0019	522
2500	60	800	625	32.62	0.0129	77
2500	90	100	625	4.57	0.0029	348
2500	90	800	625	32.62	0.0194	52

Table 1
θ, λ and K for a shallow reflector.

In **Table 2** the same comparisons are made, but with a reflector at a depth of 1500 m with velocities of 4000 m/s, as we vary the frequencies from 10 to 90 Hz and the offsets from 200 to 2200 m.

V (m/s)	f (s^{-1})	X (m)	D (m)	θ	k_{app} (m^{-1})	λ_{app} (m)
4000	10	200	1500	3.81	0.0002	6013
4000	10	2200	1500	36.25	0.0015	676
4000	30	200	1500	3.81	0.0005	2004
4000	30	2200	1500	36.25	0.0044	225
4000	60	200	1500	3.81	0.0010	1002
4000	60	2200	1500	36.25	0.0089	113
4000	90	200	1500	3.81	0.0015	668
4000	90	2200	1500	36.25	0.0133	75

Table 2

θ, λ and K for a deeper reflector.

The previous tables are used to determine the apparent wavelengths of signal that one can expect. Unfortunately, seismic data is a mixture of signal and noise, and then we should also determine the apparent wavelengths for air blast and ground roll (**Table 3**). Air blast has all frequencies and it is safe to assume a velocity equal to 330 m/s. Ground roll has dominant frequencies in the range of 5 – 25 Hz. It travels parallel to the surface with a velocity range between 200 and 500 m/s approximately.

Air blast				Ground roll			
v (m/s)	f (s^{-1})	λ (m)	k (m^{-1})	v (m/s)	f (s^{-1})	λ (m)	k (m^{-1})
330	10	33.00	0.030	200	5	40	0.025
330	20	16.50	0.061	200	10	20	0.050
330	30	11.00	0.091	200	15	13	0.075
330	50	6.60	0.152	200	20	10	0.100
330	60	5.50	0.182	200	25	8	0.125
330	70	4.71	0.212	500	5	100	0.010
330	80	4.13	0.242	500	10	50	0.020
330	90	3.67	0.273	500	15	33	0.030
330	100	3.30	0.303	500	20	25	0.040
330	200	1.65	0.606	500	25	20	0.050

Table 3

λ and K for air blast and ground roll.

From these tables some basic observations can be made. For a same depth and frequency, the angle of emergence increases as the offset increases; also the apparent wavenumber increases as the angle of emergence increases. For a same offset and depth, the apparent wavenumber increases with frequency. The wavenumbers for a deeper reflector are smaller than the ones for a shallow reflector. In the signal range, the shallow far offsets have the largest wavenumbers (smaller wavelengths). Seismic signal wavenumbers are in the range between 0 and 0.02 m^{-1}, this range could get slightly higher if the zone of interest is shallower and has higher frequencies. Ground roll has a limited range of small wavenumbers where it exists, from 0.010 m^{-1} to a

maximum in some cases of 0.125 m^{-1}, and the air blast has a broader range varying from 0.020 m^{-1} to about 0.7 m^{-1}. In **Figure 3** these wavenumbers are illustrated with air blast in red, ground roll in yellow and signal in blue. The orange and green show areas in which the wavenumbers are mixed. **Figure 4** is a detail of the signal-noise interaction zone. It can be seen that the most limiting range in which the signal is going to mix with the noise is at the far-offsets shallow reflections.

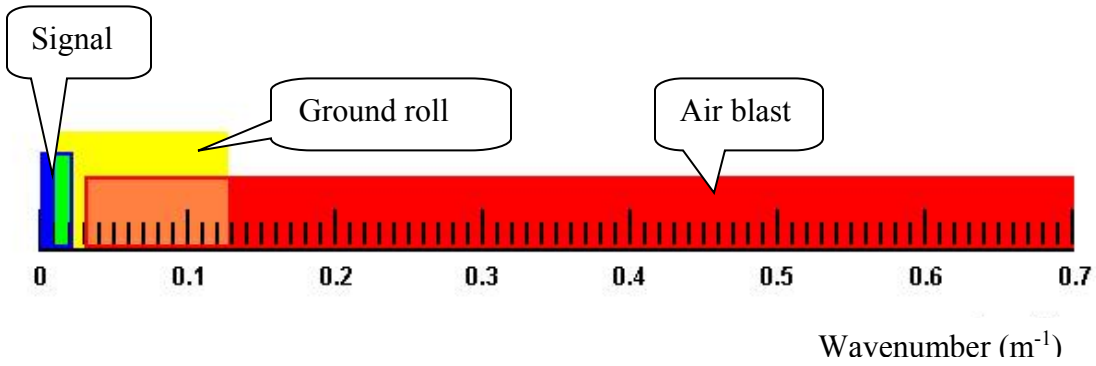

Figure 3
Air blast, ground roll and signal wavenumbers interaction.

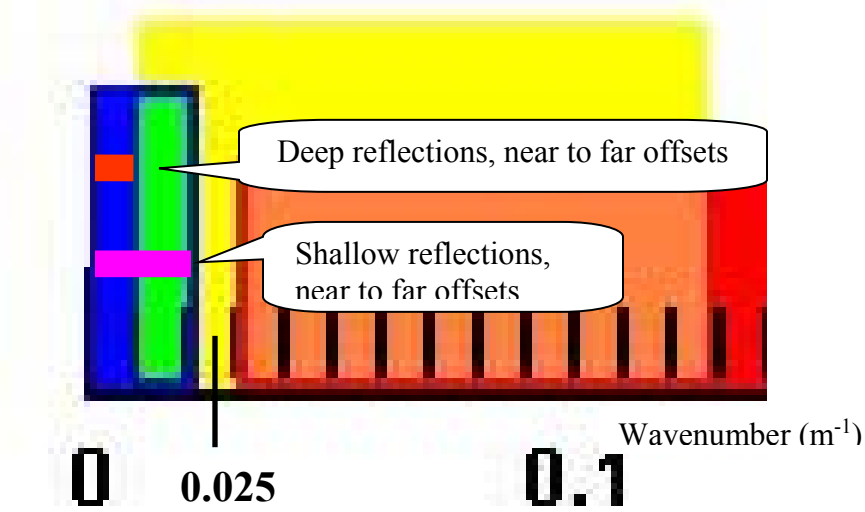

Figure 4
Wavenumber overlap.

These observations are very important because if we are to design an array to attenuate noise, it should filter the wavenumbers beyond the signal bandwidth. To determine the number of geophones and the spacing

required for a linear array to attenuate any given range of apparent wavelengths one needs to know (Cooper, 2005):

λ_{pro}= the shortest wavelength wanted to protect
λ_L = longest wavelength desired in the reject zone
λ_S = shortest wavelength desired in the pass band
Then the effective array length (L_E) required is equal to:

$$L_E = N \times S = \lambda_L = \lambda_{pro}/2 \quad (4)$$

where N, the number of elements in the array is equal to:

$$N = L_E / (\lambda_S + 1) \quad (5)$$

and S, the spacing between elements is :

$$S = L_E / N \quad (6)$$

What are the reject zone and the pass band? To explain these concepts **Figure 5** will be used. This figure depicts the array response of a nine-element array represented in attenuation (dB) versus wavenumber (m^{-1}). There are a total of 7 whole lobes plus 2-half lobes in the graph, and this is equal to the number of elements in the array. The last lobe on the right side is called the first repeat. The first lobe describes the pass band, and it contains the longest wavenumbers of signal we need to protect with minimum attenuation. The array response curve is generated using equation (7):

$$R(k) = 20 \, \mathrm{Log}\left(\frac{\sum_{i=1}^{M} w_i \cos\left(2\pi k \left(d_i - d_c\right)\right)}{\sum_{i=1}^{M} w_i} \right) \quad (7)$$

where:

R(k) = response in dB at wavenumber k
k = wavenumber
w_i = relative weight of i^{th} element of the array
d_i = distance of the i^{th} element from an arbitrary reference point
d_c = distance of the array center from the same reference point
M = total number of weights in the array

There is a reject zone that exists between the first and last notch. Any information that lies in this area will be rejected, and the maximum attenuation is reached at the notches. Each one of the lobes has attenuation, forming a lobe envelope that is determined with the following equation (Brian Evans, 1997):

$$\text{Lobe envelope} = 20 \, \mathrm{Log}\left(\frac{1}{N}\right); \text{ N: 1, 2, 3 .. n-1} \quad (8)$$

The equations used to determine the notches and peaks are:

$$\text{Notch} = \frac{N}{L_E}; \quad \text{N: 1, 2, 3 …….. n-1} \quad (9)$$

$$\text{Peak} = \frac{N + 0.5}{L_E};\ \text{N: 1, 2, 3 …….. n-1} \qquad (10)$$

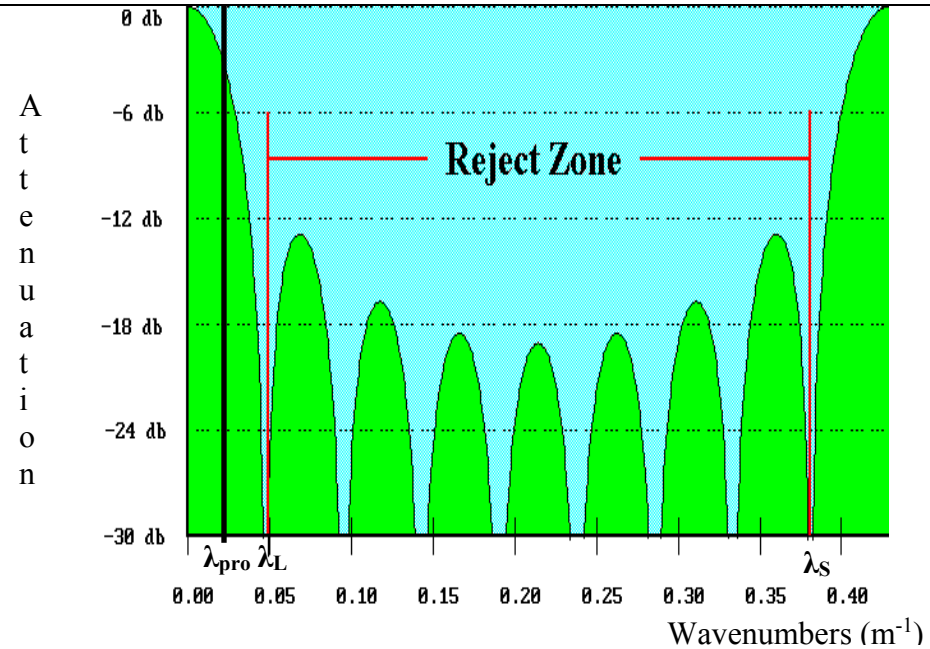

Figure 5
Array response for a 9-element group interval.

Gijs Vermeer (Vermeer, 1990) in his classic 3-D symmetric sampling paper makes the following definitions:

the pass band is equal to $|k| < 1 / L_E$ (11)

the reject band is equal to $1 / L \leq |k| \leq (N-1) / L_E$ (12)

and the aliased pass band is equal to $(N-1)/L_E < |k| < (N+1)/L_E$ (13)

With the background review completed, let us study some publications.

1. ANALIZING THE EFFECTIVENESS OF RECEIVER ARRAYS FOR MULTICOMPONENT SEISMIC EXPLORATION. (Hoffe et al, 2002)

The purpose of this paper is to demonstrate through a case history the little benefit of receiver arrays when compared to point receivers. In the Blackfoot oil field of Alberta, a 3 Km 3C 2-D line is acquired with conventional 20 m shot and receiver intervals at the end of the line, and with high-resolution parameters of 20 m source intervals and 2 m receiver interval in the center of the line.

Two array design approaches are studied and compared to point receivers. In the noise-aggressive approach the effective length of the array is equal to two times the receiver interval ($L_E=2\Delta G$). The signal-preferred array approach has an effective array length equal to the group interval ($L_E=\Delta G$). The authors do a trace-summation process to form the arrays by convolving a space series of 1's and 0's at 2-m spatial sampling, where the 1's represent the geophones in the arrays, with the vertical and radial component source gathers.

The parameters for the arrays used in this study are shown in **Table 4** and their responses are shown in **Figure 6**. As it can be seen, both arrays have the same Nyquist wavenumber, but where the ΔG array has a lobe in the Nyquist value, the $2\Delta G$ array has a notch. Using the vertical dashed line described by $K_{NG} = 0.05$ m^{-1} (Nyquist for the group interval), one can see that the ΔG array is called the signal-preferred approach because it has a wider pass band, and the $2\Delta G$ array is called the noise-aggressive approach because of its narrow pass band.

Group Interval (m)	Number of elements	Receiver spacing (m)	Array effective length (m)	1st reject notch (m^{-1})	K_{Ny} (m^{-1})	Last reject notch (m^{-1})	Aliased pass band (m^{-1})
20	5	4	20	0.05	0.125	0.20	0.25
20	10	4	40	0.025	0.125	0.225	0.25

Table 4
ΔG and $2\Delta G$ arrays.

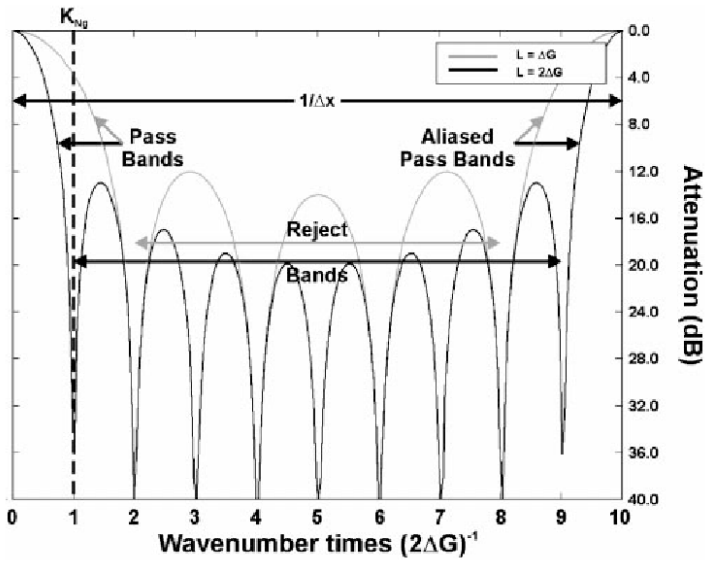

Figure 6
ΔG and $2\Delta G$ array responses.
Taken from (Hoffe et al, 2002)

P-P and P-S data were analyzed in a variety of domains. In **Figure 7** the vertical shot gathers and the F-K spectra with array responses are compared for the point receiver, 5-element (ΔG) and 10-element (2ΔG) arrays, and in **Figure 8** the radial shot gathers are analyzed. These figures demonstrate the effect of trace summation, in which the traces from the high-density survey were convolved with a space series that represent the receiver locations. In both figures, plots (a) and (b) show the t-x and F-K plots for the point receivers, plots (c) and (d) show the t-x and F-K plots for the 5-element array and plots (e) and (f) show the t-x and F-K plots for the 10-element array. In the t-x domain there is some improvement in the continuity of the reflection events on both array gathers due to the suppression of air blast and ground roll. In the F-K domain the 10 element array provides more attenuation. More importantly, note how the signal is attenuated with the 10-element array.

After the trace summation, a downsampling is executed to simulate group intervals of 20 meters. In **Figure 9**, the downsampled vertical gathers are depicted. Plot (a) shows the original point receivers. Plot (b) depicts the point receivers downsampled to 20 m showing aliasing in the near offsets. Plot (c) illustrates the 5-elemnet array and (d) the 10-element array. Even though in the paper both array gathers are said to have less aliasing, in my opinion, they look pixilated and not aliased, and some noise reduction is also observed. In **Figure 10** the F-K spectra can be compared. As in the previous figure, plot (a) show the high-density point receiver, plot (b) the downsampled point receiver, plot (c) the 5-element array and plot (d) the 10-element array. None of the downsampled F-K spectra look as good as the original point receiver, and all of them show wrap-around effect, but in the array plots (c) and (d), the main energy is not aliased.

Similar comments can be made for the downsampled radial gathers shown in **Figure 11** and their F-K spectra in **Figure 12**. The same plot order used in the 2 previous figures is used. All three downsampled P-S gathers look more pixilated than the P-P gathers which might be an indicative that smaller sample intervals may be required for P-S data.

Figure 13 depicts portions of the unmigrated P-P stacks for the downsampled point receiver (a), 5-element array (b) and 10-element array (c). These stacks are very similar with subtle differences. **Figure 14** shows portions of the unmigrated P-S stacks with plots (a), (b) and (c) describing the same stacks as in the P-P case. Less amplitude, coherency and continuity of events in the array formed stacks can be seen, especially in the 10-element array. Due to these observations the authors concluded that arrays are detrimental to P-S data.

Spectral analyses of amplitude and phase coherency are carried out for the P-P (**Figure 15**) and the P-S (**Figure 16**) stacks in the F-X domain. For both figures, plot (a) represents the f-x amplitude spectrum for the point receiver, (b) the corresponding f-x phase spectrum, plot (c) shows the f-x amplitude spectrum for the 5-element array, (d) its corresponding f-x phase spectrum, plot (e) illustrates the f-x amplitude spectrum for the 10-element array and plot (f) the corresponding f-x phase spectrum. In both cases the authors interpreted a consistent decrease in signal with increasing array length, being more severe in the P-S case.

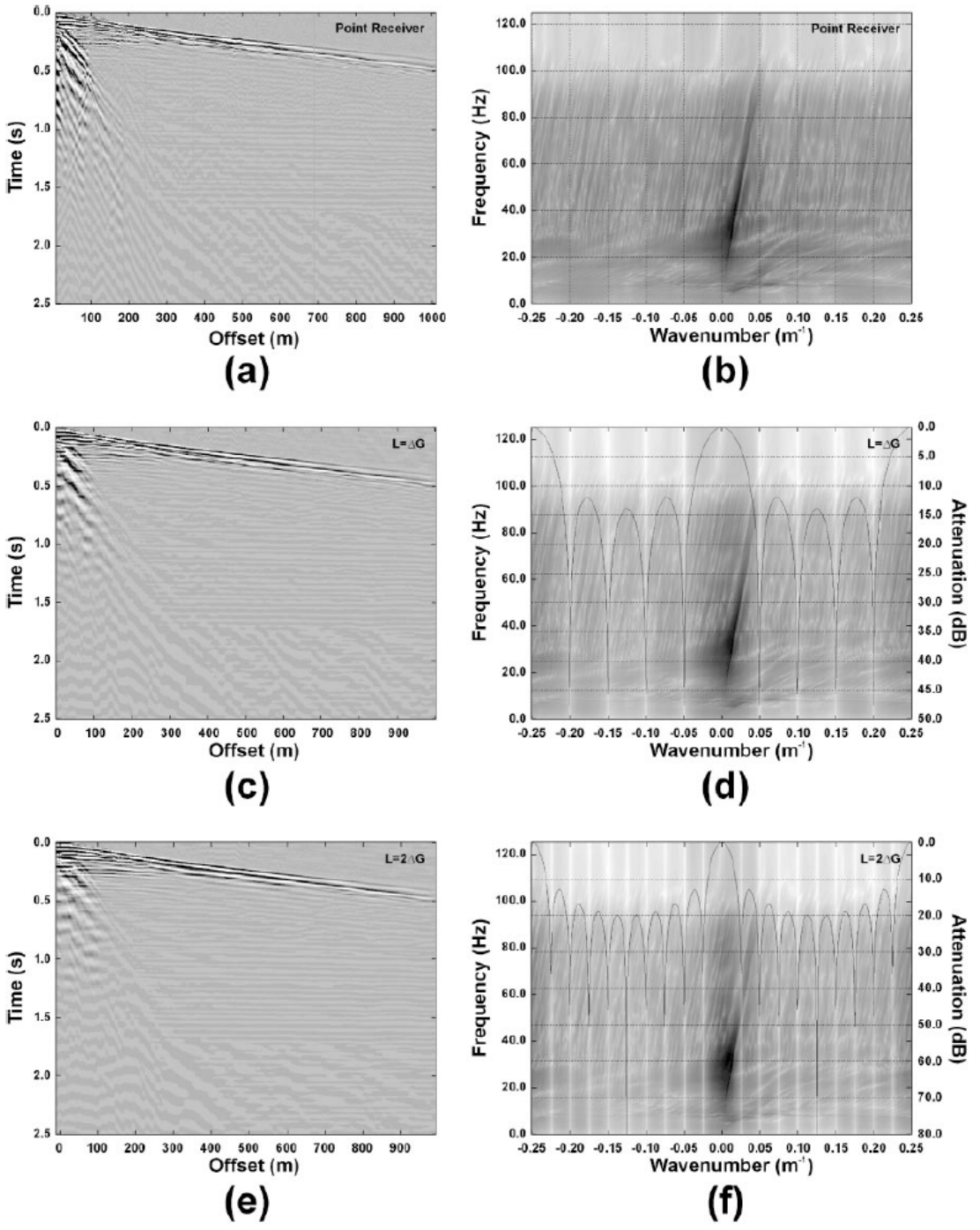

Figure 7
P-P shot gathers and F-K plots for point receivers, ΔG and 2ΔG arrays.
Taken from (Hoffe et al, 2002)

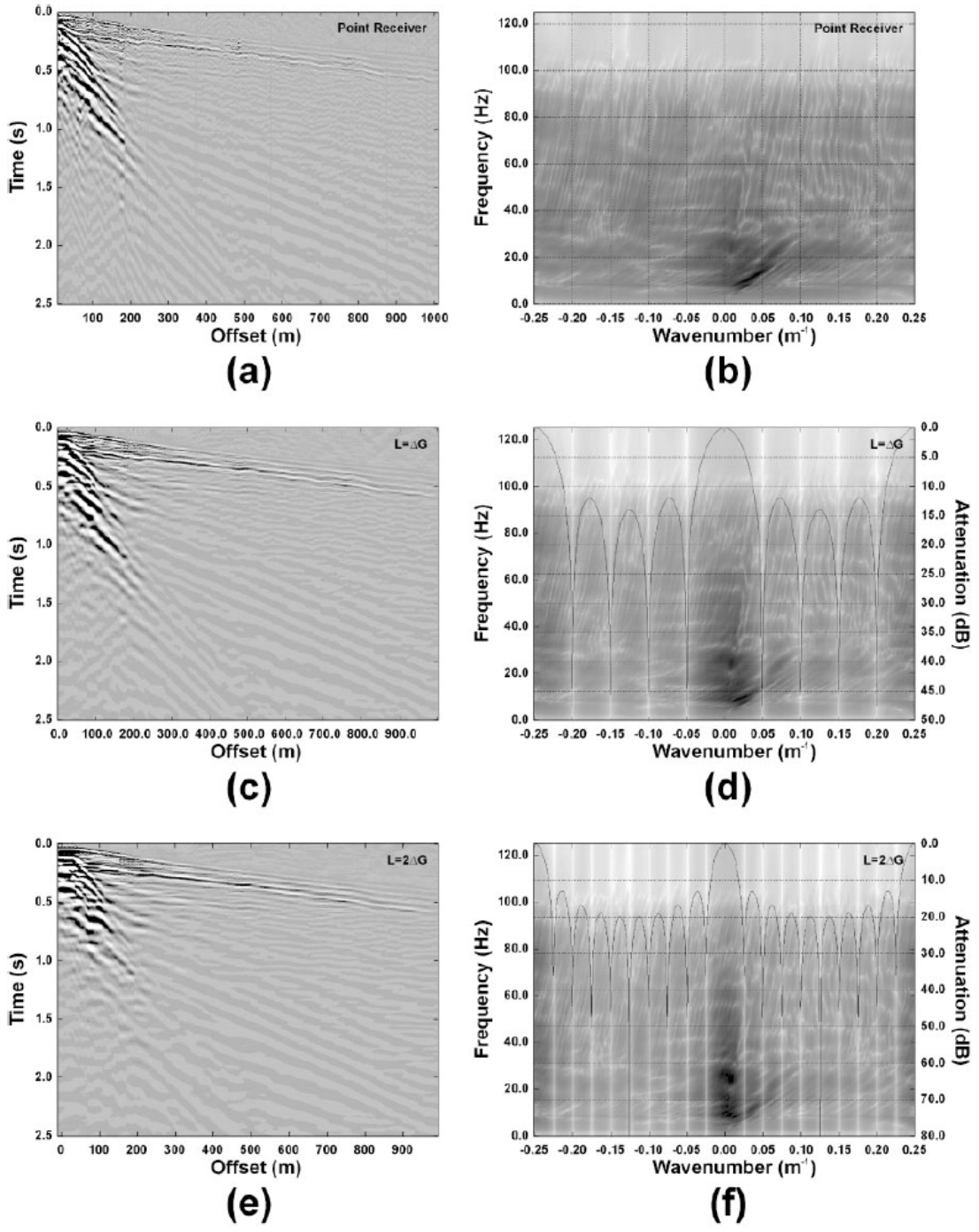

Figure 8
P-S shot gathers and F-K plots for point receivers, ΔG and 2ΔG arrays.
Taken from (Hoffe et al, 2002)

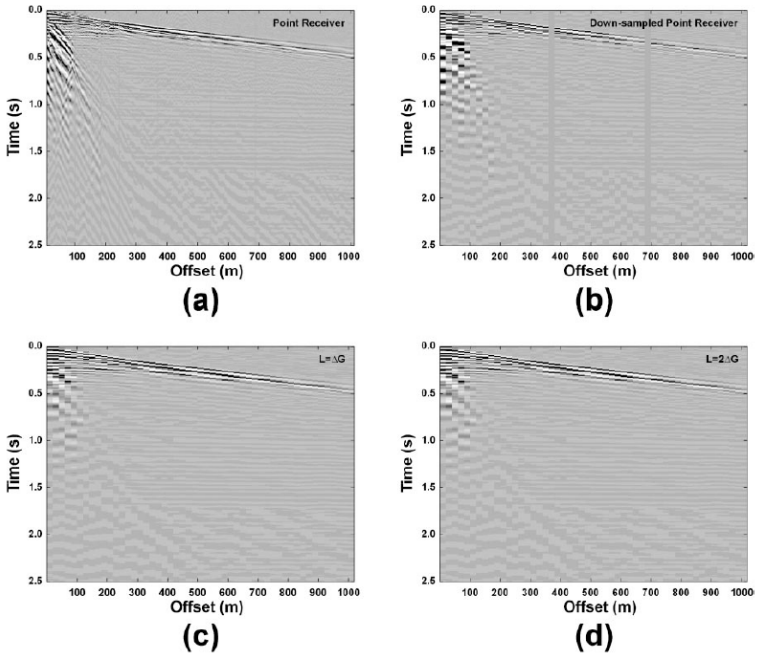

Figure 9
Vertical shot gather downsampling in t-x domain.
Taken from (Hoffe et al, 2002)

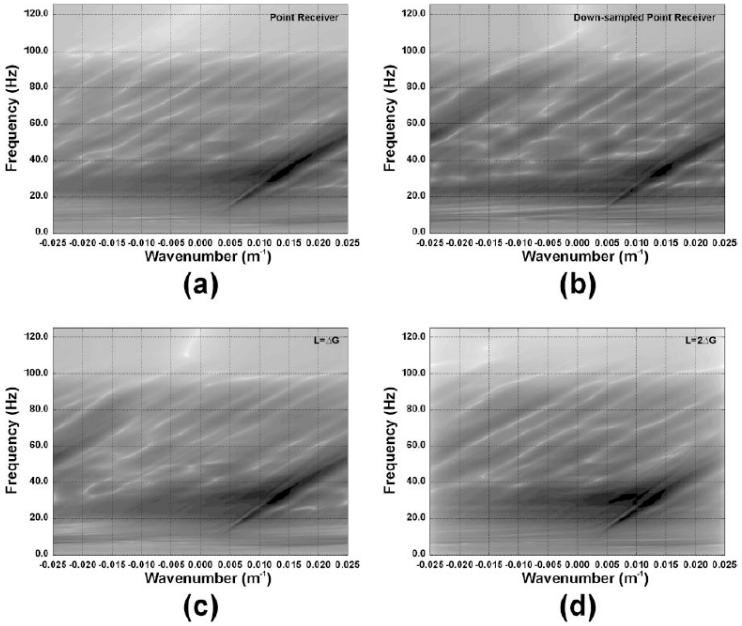

Figure 10
Vertical shot gather downsampling in F-K domain.
Taken from (Hoffe et al, 2002)

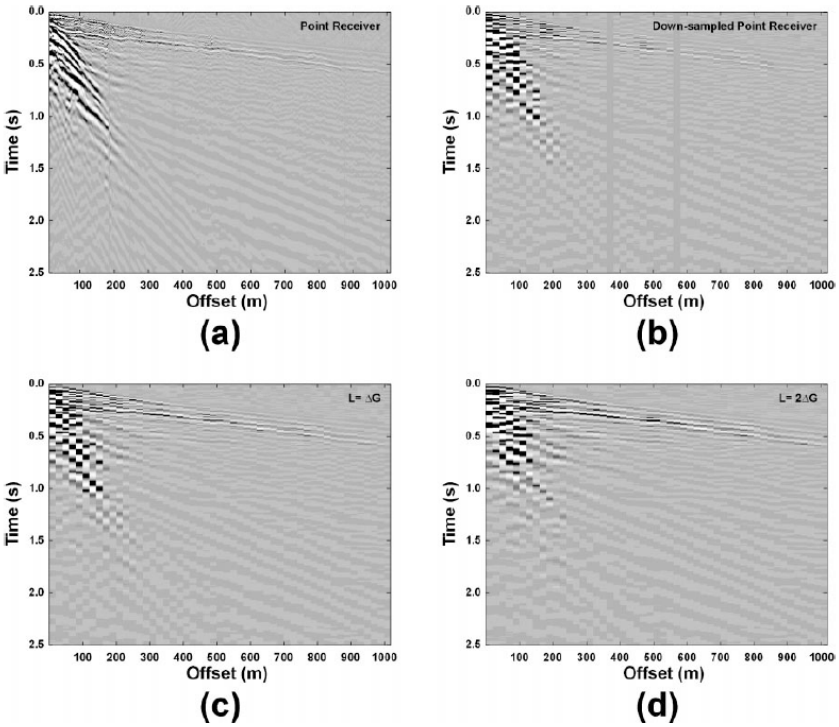

Figure 11
Radial shot gather downsampling in t-x domain.
Taken from (Hoffe et al, 2002)

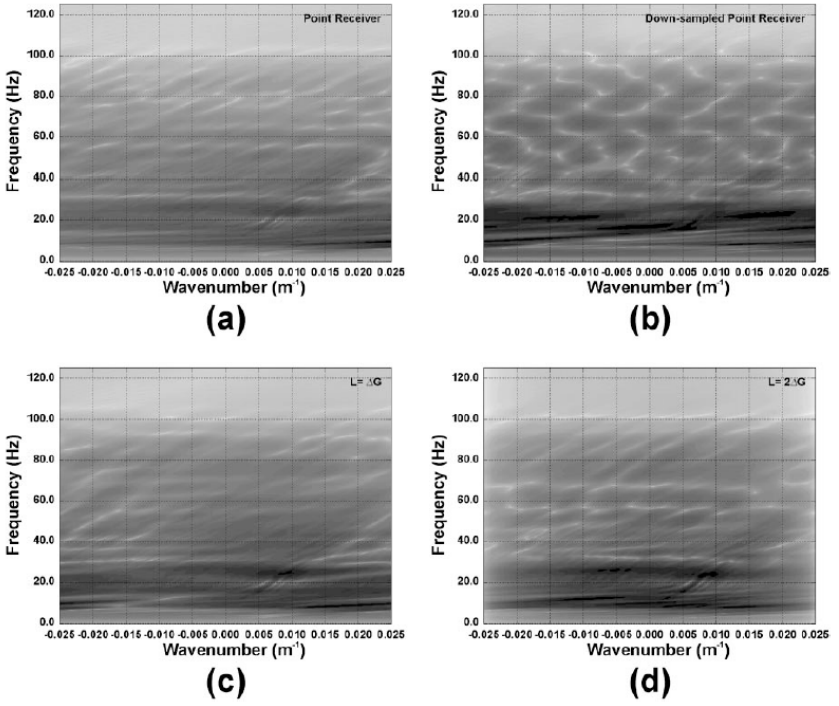

Figure 12
Radial shot gather downsampling in F-K domain.
Taken from (Hoffe et al, 2002)

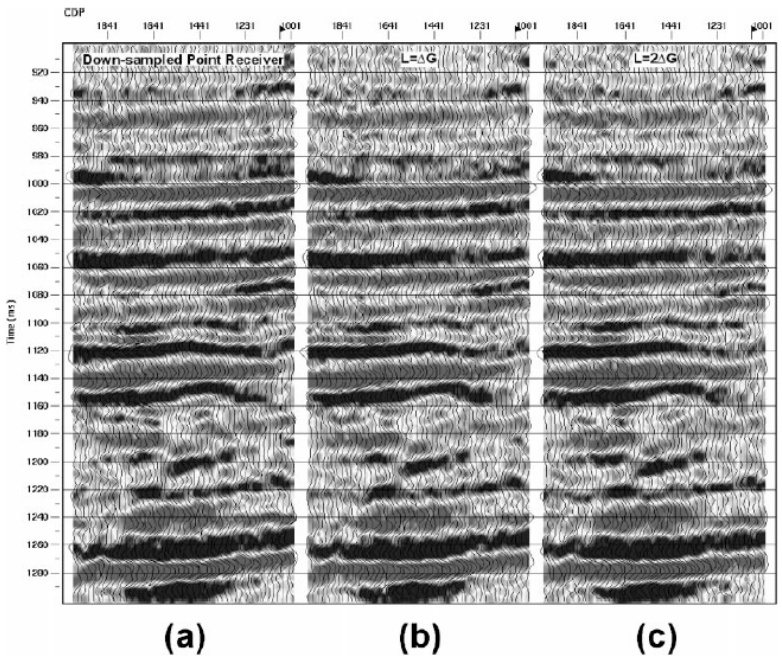

Figure 13
Portions of final unmigrated P-P stacks.
Taken from (Hoffe et al, 2002)

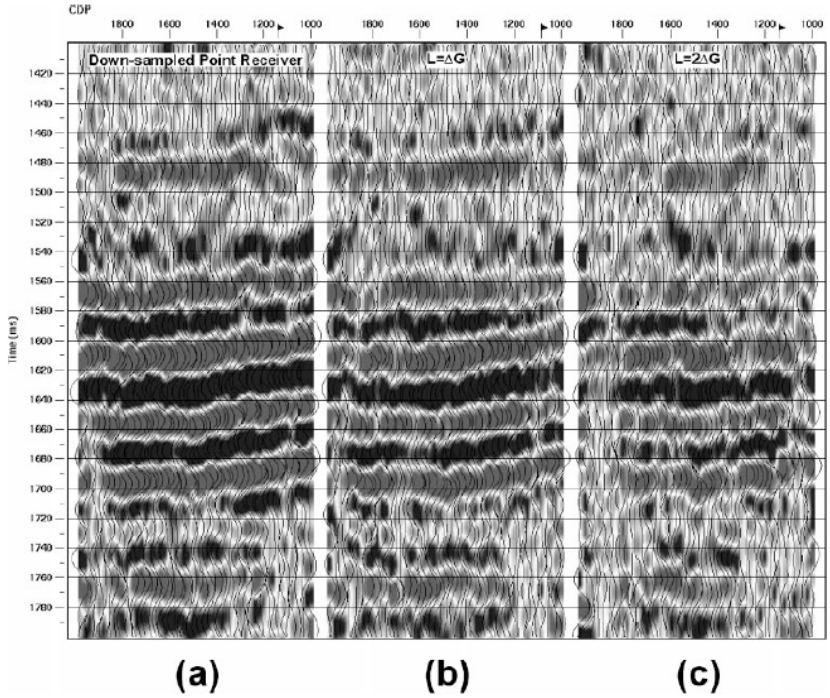

Figure 14
Portions of final unmigrated P-S stacks.
Taken from (Hoffe et al, 2002)

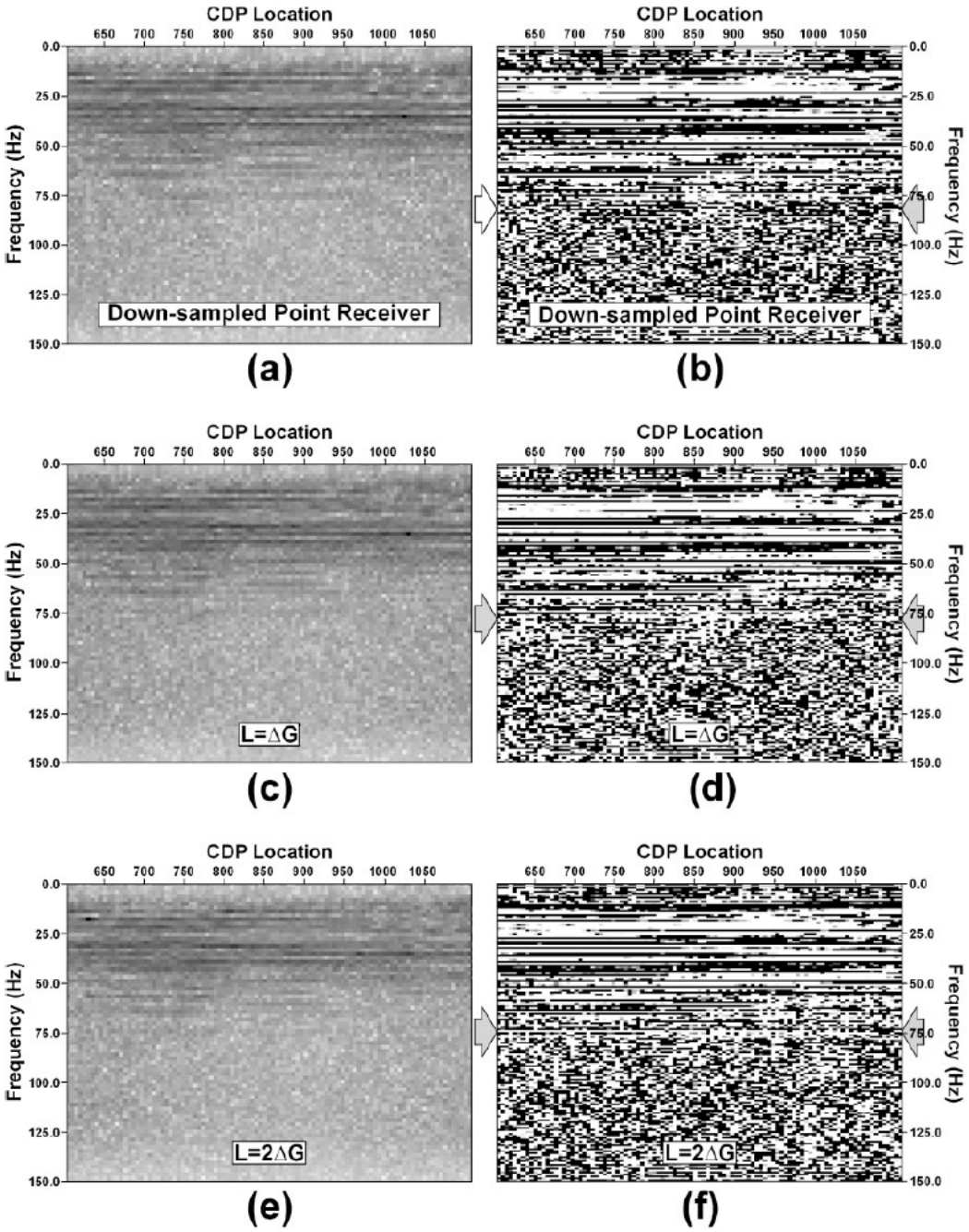

Figure 15
Poststack spectral analyses of the vertical stacks.
Taken from (Hoffe et al, 2002)

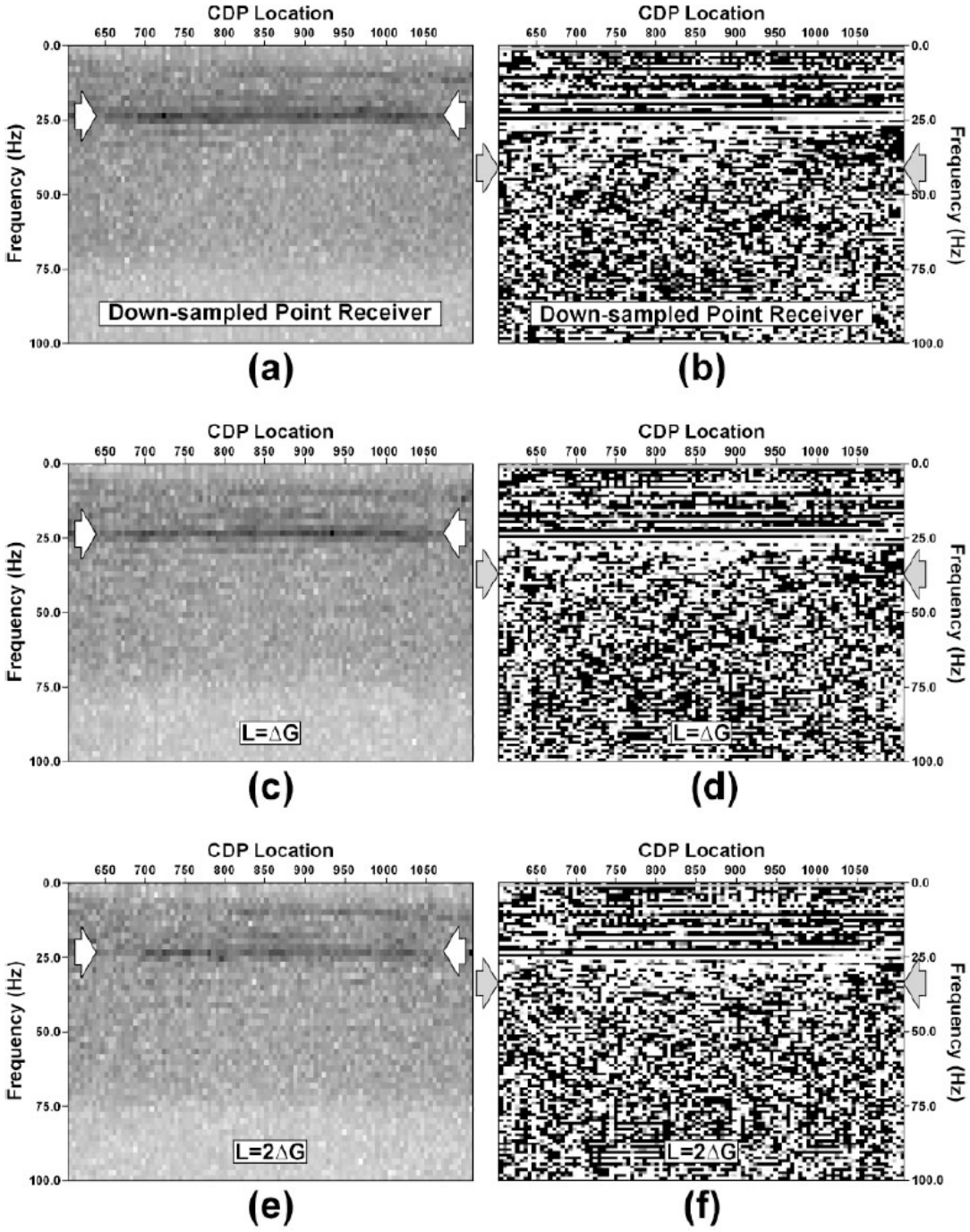

Figure 16
Poststack spectral analyses of the radial stacks.
Taken from (Hoffe et al, 2002)

In **Figure 17** the average amplitude spectra for the P-P stacks shows that above 40 Hz there is a higher power for the point receiver stack. The ΔG and 2ΔG arrays have very similar behaviors with the ΔG array outperforming the 2ΔG above 48 Hz. In **Figure 18** for the P-S amplitude spectrum similar conclusions can be reached, being the 2ΔG array the one with the worst performance having the greatest loss of 4.5 dB around 25 Hz.

The authors discussed what might have caused the poor quality P-S stacks, and they mentioned intra-array statics as the cause. They reprocessed the data, applying refraction, residual and trimmed statics to the traces within the arrays and significant improvement is achieved (**Figure 19**). All the plots describe statics applied prior to array simulation. Plot (a) is the P-S stack with no statics applied, in plot (b) the refraction statics were applied, in plot (c) refraction and residual statics were applied, and in plot (d) refraction, residual and trim statics were applied. Note the improvement in amplitudes and coherency with every step.

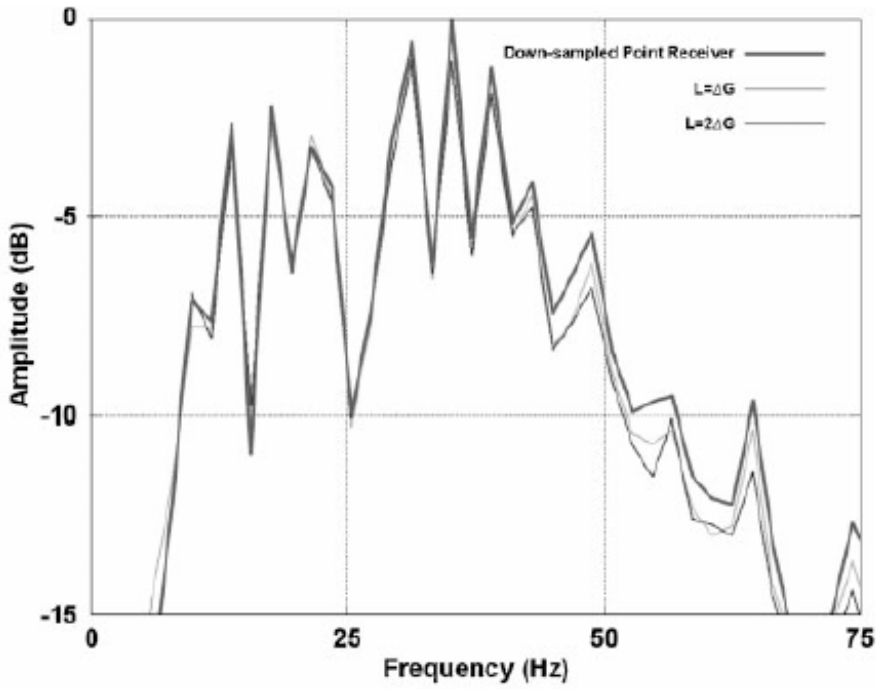

Figure 17
P-P amplitude spectra for the 0-75 Hz range.
Taken from (Hoffe et al, 2002)

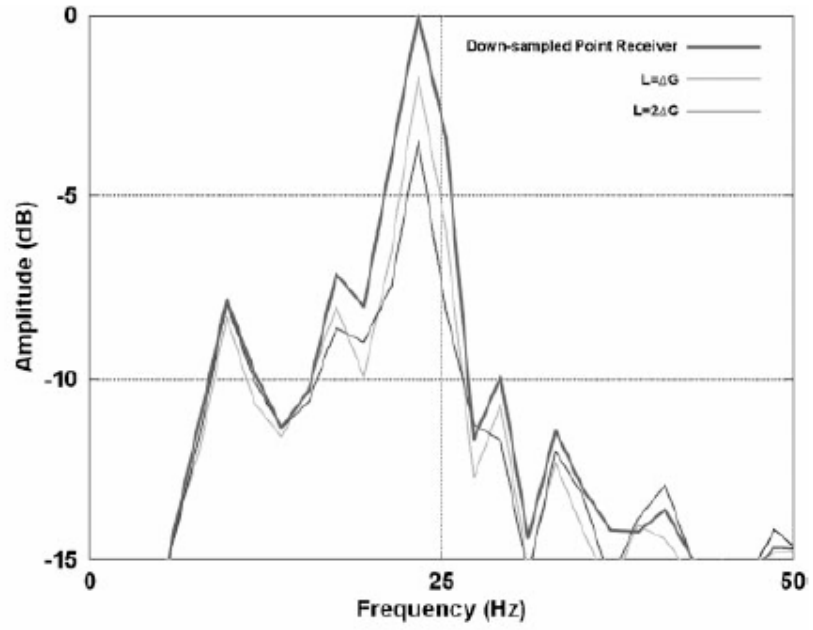

Figure 18
P-S amplitude spectra for the 0-50 Hz range.
Taken from (Hoffe et al, 2002)

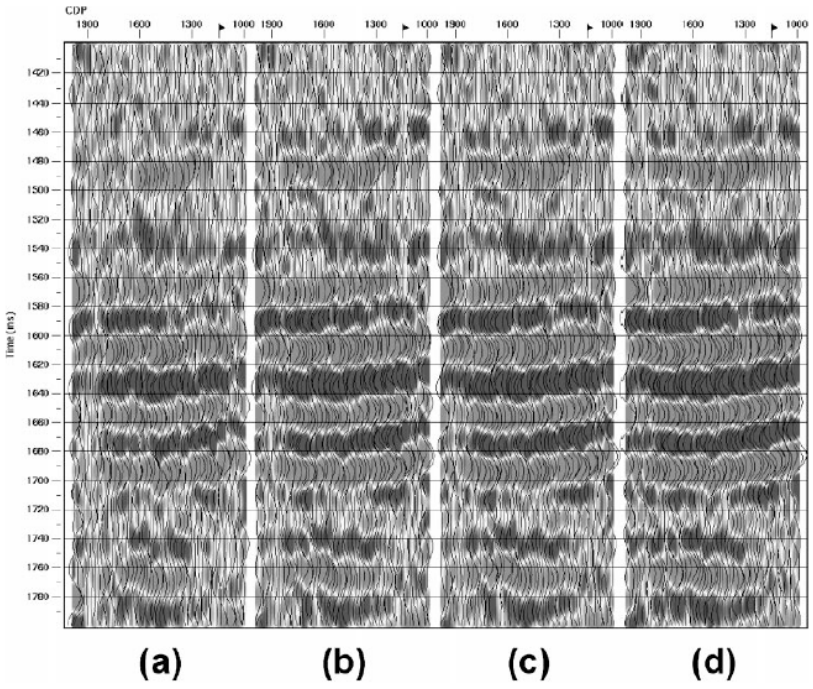

Figure 19
2ΔG array data reprocessed.
Taken from (Hoffe et al, 2002)

The authors concluded that both arrays showed ability to suppress coherent noise and acted as anti-alias filters, with the 10-element array being superior. They also concluded that neither array improved the quality of the final stacked section when compared to the downsampled point receiver one. For the P-P case subtle differences were observed, but in the F-X analysis, signal band loss with increasing array length was seen. In the P-S case the deterioration is evident in the stacks and in signal loss with greater array lengths.

This paper is one of the best amongst all the papers selected for this report. The array simulations were well conducted as well as the analysis of the data. These conclusions are applicable only for the area of study and should not be generalized. There are other areas where the coherent, incoherent and random noises present a difficult problem and arrays are appropriate tools to deal with them. I agree with Vermeer (Vermeer, 2003) when he said that to not deteriorate the P-S waves a smaller receiver interval should be used. For the P-S data, he also states that arrays should not be used and that the noise should be suppressed in processing.

2. PATTERNS – WITH A PINCH OF SALT (Newman et all, 1973)

Newman and Mahoney wrote in 1973 a paper that can be classified as a "Classic". A seismic array is a wavenumber filter that gets influenced by implementation errors in the space domain. The purpose of this paper is to investigate the changes in array performance as a result of implementation errors.

The variables at the array designer's disposal are the element weights, element position and total number of elements. The designer has two options when designing an array: to vary the weights of uniformly spaced elements, or to vary the linear density of equally weighted elements.

The authors classified arrays into four types:

- The uniform array: the elements have the same weight and are distributed uniformly along a straight line. The Fourier transform of the response is described by the Sinc function (sin x/x).
- Linearly tapered array: successive elements in a linearly increasing fashion towards the array center. The elements distribution has a triangular shape and its Fourier transform is described by $\sin^2 x / x^2$.
- Savit arrays: the response is best fit in a least-squares sense to the ideal low pass requirement. The shape of the elements distribution in these arrays resembles a half moon.
- Chebyshev array: the array weights are constrained so that successive side lobes in the reject zone have equal

magnitude are minimized. The element distribution follows a Gaussian curve.

Savit and Chebyshev arrays are more efficient than uniform and linearly tapered arrays because they provide greater attenuation over a broader bandwidth with same number of elements.

Array design follows two assumptions: a plane wave propagating at uniform apparent velocity through the array, and that each element responds to the same seismic disturbance, but with appropriate time delays. The errors in design introduced by theses assumptions are the curvature of the wavefronts, the amplitude decay across span of array and the static time corrections. There are also errors in implementation: the element response, non-vertical plants, element positioning, ground coupling and the local heterogeneities beneath the surface.

The authors modeled all these errors by modifying the element weights and positions. The procedure consisted of modifying the array response a total of 50 times, in which the variable (weight or position) was affected randomly within a 10 % standard deviation using a Gaussian distribution. Then the mean array response is analyzed.

In **Figure 20**, the plot on the left represents a uniform array response, the one in the center shows the 50 repetitions with random errors in weight of 10 % standard deviation, and the one on the right is the mean. The response of the uniform array is least affected by errors in weight. The response of the pass band does not change much, and the side lobe responses are very similar to the nominal case. Note that the large attenuation obtained in the nominal case (more than 100 dB loss) gets limited to 32 dB in the mean.

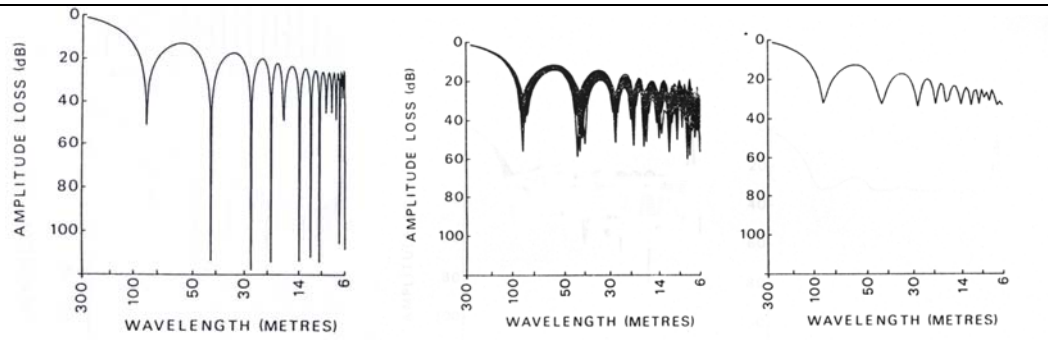

Figure 20
Uniform array responses: nominal (left), 50 errors repetitions (center) and mean (right). Taken from (Newman et al, 1973)

In **Figure 21**, **Figure 22** and **Figure 23** the plot on the left represents nominal array response, the one in the center shows the 50 repetitions with random errors in weight of 10 % standard deviation, and the one on the right is the mean, for linearly tapered, Savit and Chebyshev arrays respectively. The behaviors of these arrays are comparable in that when

analyzing the rejection zones, they look very different to the nominal case. Note that in all the cases the mean attenuation was weak when compared to the nominal cases.

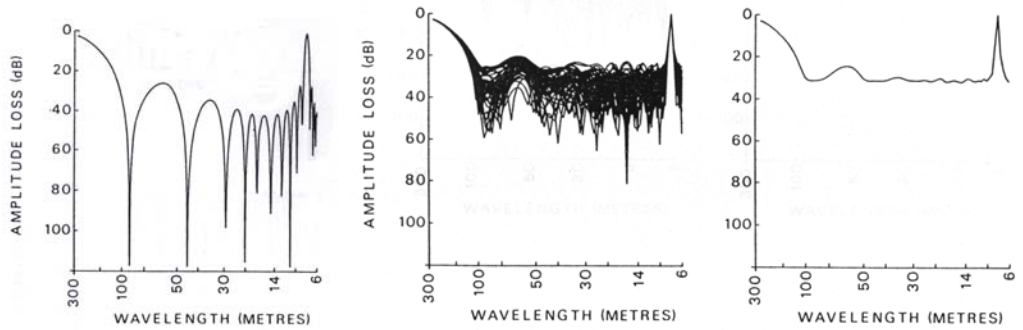

Figure 21
Linearly tapered array responses: indiv. (left), 50 errors repet. (center) and mean (right).
Taken from (Newman et al, 1973)

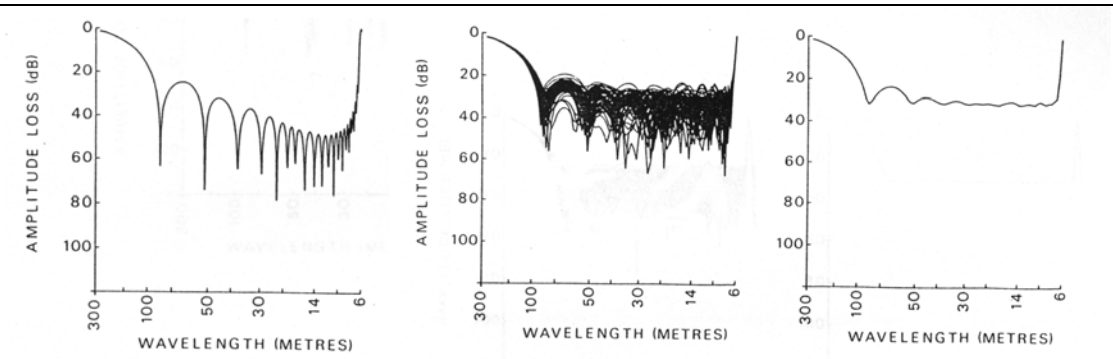

Figure 22
Savit array responses: individual (left), 50 errors repetitions (center) and mean (right).
Taken from (Newman et al, 1973)

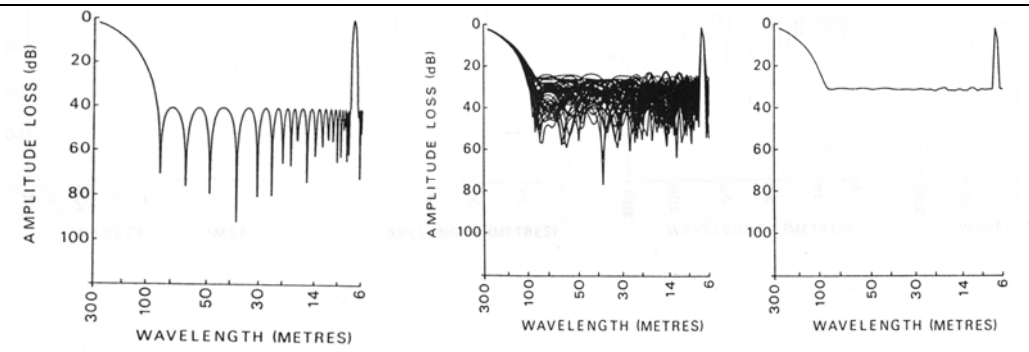

Figure 23
Chebyshev array responses: indiv. (left), 50 errors repet. (center) and mean (right).
Taken from (Newman et al, 1973)

The effect of random errors in weight, impose a limit in the maximum attenuation achieved. In the presence of errors, the distribution of weights can be considered as the sum of two distributions: the nominal and the error sequence distribution. Using Fourier theory, when the error sequence is transformed, it has a uniform amplitude response that will be a threshold level of attenuation and the array response cannot fall below it.

An experiment was run with three Chebyshev arrays with similar reject bands and element spacing, and different weights and number of elements, in order to obtain a nominal attenuation level of 20, 40 and 60 dB. **Figure 24** shows the mean results after running fifty arrays with errors in weight of 2, 5, 10 and 20 % standard deviation. The 20 dB nominal curve is the least affected by errors. The 60 dB nominal curve is very sensitive to errors. When the error increases, the attenuation decreases and these observations are made independently of array type.

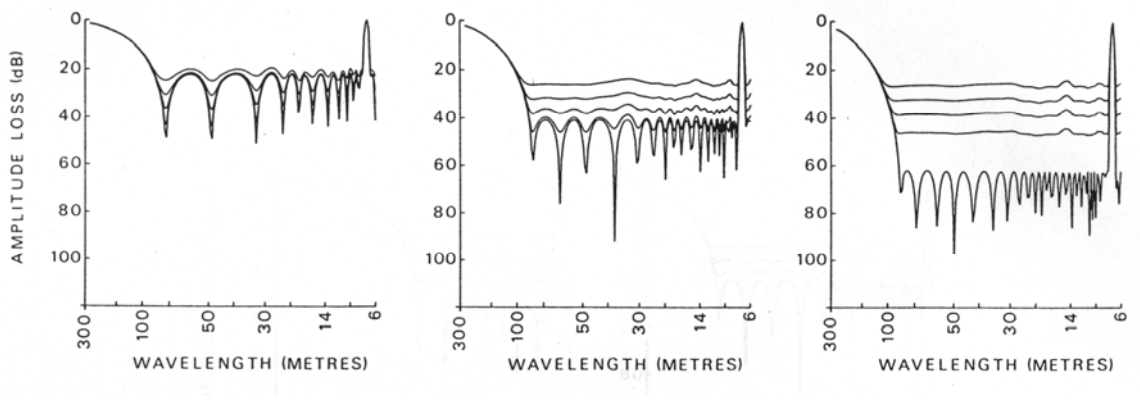

Figure 24
Nominal attenuation of 20 (left), 40 (center) and 60 (right) dB- errors in weight-.
Taken from (Newman et al, 1973)

The following series of experiments show the mean of 50 array responses in which the errors in position had 2, 5, 10 and 20 % standard deviation. **Figure 25** illustrates the 20, 40 and 60 dB Chebyshev arrays. The effects of errors in position are similar to those of errors in weight. The limit of attenuation is related to the magnitude of position error.

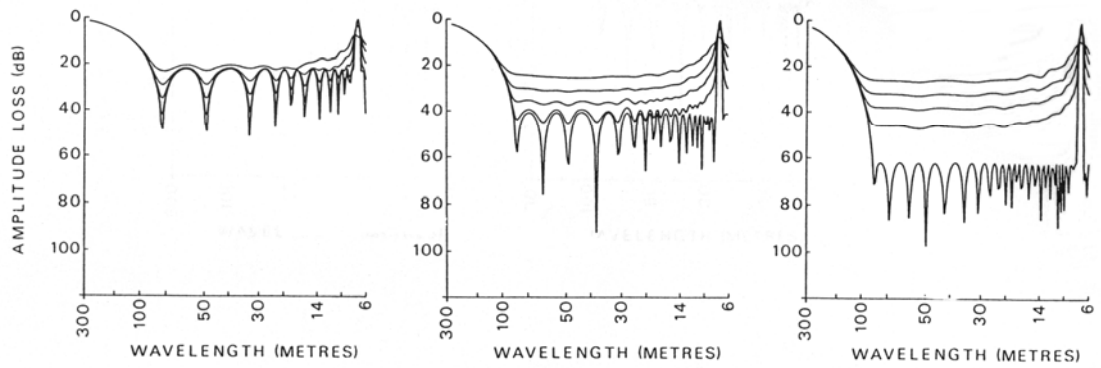

Figure 25
Nominal attenuation of 20 (left), 40 (center) and 60 (right) dB- errors in position-. Taken from (Newman et al, 1973)

The rejection capabilities of an array have a limit imposed by the error implementation errors. From the experiments, it can be learned that the threshold level of attenuation is inversely proportional to the standard deviation error, directly proportional to the square root of the number of elements in the array, and independent of array type. An infinite attenuation is never obtained with errors.

The authors suggest that two approaches can be taken when combined source and receiver array performance is inadequate. First, increase source offset or vary source depth. Second, increase the number of elements in the array by reducing the geophone separation (preserving the same array length) and therefore, the attenuation limit is improved by $\sqrt{n}$.

In 1973, deconvolution was not studied as it is nowadays, and the suggestion of varying the hole depth was appropriate in those years. Nevertheless, we know that even though the ghost can act as an array, increasing the hole depth decreases the pass band width. If the ghost period is smaller than the decon operator, the trace is stabilized, but if it is longer, the ghost gets propagated.

3. EVALUATION OF SEISMIC FIELD ARRAYS IN THE TEMPORAL FREQUENCY DOMAIN (Rigdon et al, 1987)

Rigdon et al introduce a method of evaluating arrays in the temporal frequency domain. Commonly, array responses are displayed in amplitudes versus wavelength/wavenumber. To make the conversion from spatial frequency to temporal frequency, one has to know the velocities, useable offsets and depth of the reflectors, and then apply equation (3) to evaluate the array response in amplitude versus frequency.

From **Figure 26** one can see that for a given wavelength, the high frequencies of the shallow reflectors are the most vulnerable to the array filtering effect. If one is to design an array to filter the undesired surface waves, one risks removing also the high frequencies of the shallow reflectors.

In **Figure 27** it can be seen that shallow reflectors are more sensitive to array effects than deeper reflectors. Also, the high frequency amplitudes of a shallow reflector are more vulnerable to the filtering effect than the lower frequencies. In **Figure 28** the authors experimented with different array lengths and studied the filtering effects imposed on a shallow reflector. The longer the array, the more high frequency amplitudes are lost.

Therefore, when designing an array, one has to make sure to pass the entire signal and deal with the noise later on during the processing of the data.

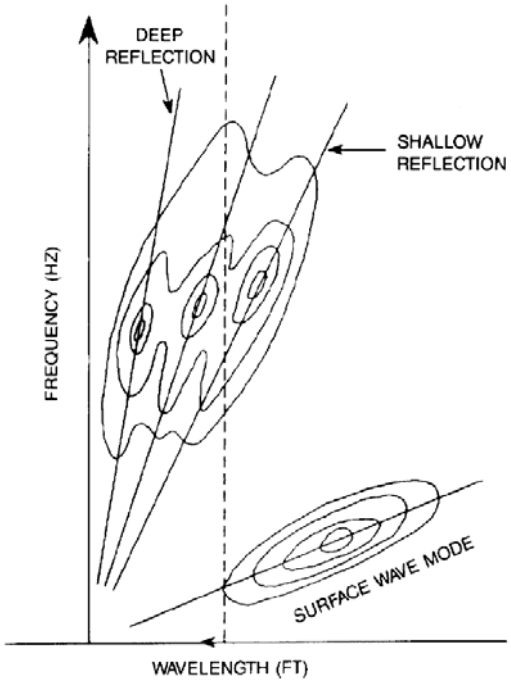

Figure 26
Separation of various energy modes in the frequency domain.
Taken from (Rigdon et al, 1987)

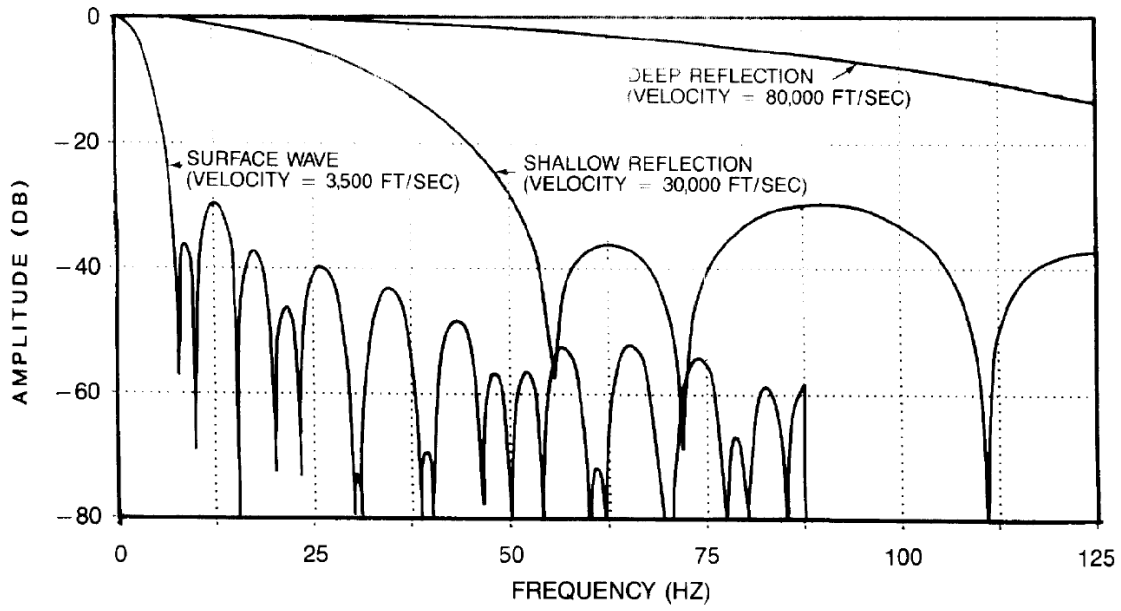

Figure 27
Array response as a function of frequency.
Taken from (Rigdon et al, 1987)

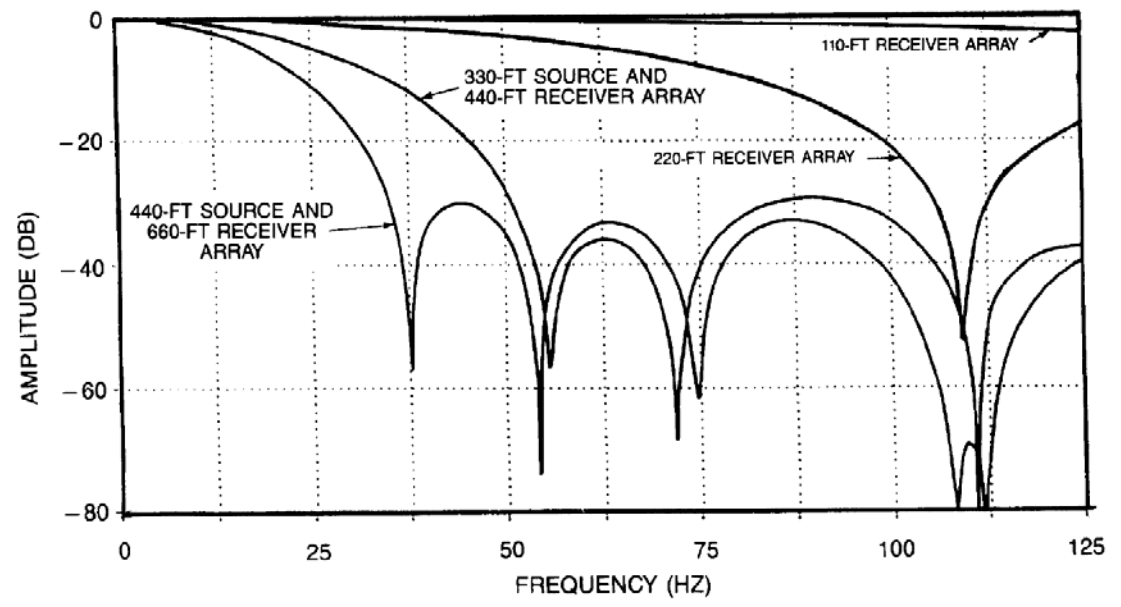

Figure 28
Shallow reflector's amplitudes versus array length.
Taken from (Rigdon et al, 1987)

4. GROUND ROLL SUPRESSION BY THE STACKARRAY (Morse et all, 1989)

During seismic data processing, there is a long array formed by summing the traces of the CMP gather. If the field geometry is such that the array is continuous and evenly spaced, then this array is called stackarray. The CMP stacking process by itself can suppress the ground roll.

When the traces (with many combinations of offsets) within a CMP are stacked, an array longer than the source/geophone field arrays is formed. This CMP array will depend on the receiver interval, source interval and length of the source/receiver arrays to suppress the ground roll appropriately.

Anstey (1986) pointed out the strategy to follow in the field so that the CMP array formed is continuous, uniformly weighted and has the same range of offsets as in the field record. The linear field array length should be equal to the spatial sampling interval. For a split-spread land acquisition, a half-integer shooting configuration should be used and the field array length would be equal to the group interval. In a end-on shooting geometry, the source interval should be equal to the receiver interval, with field arrays twice the length of the group interval.

The product of the field array and the CMP-array responses can represent the wavenumber response of the stack array. **Figure 29** shows the stack array response when the effective length of the field array and the CMP-element spacing is equal to D. Notice that where the CMP-array response has peaks, the field array has notches.

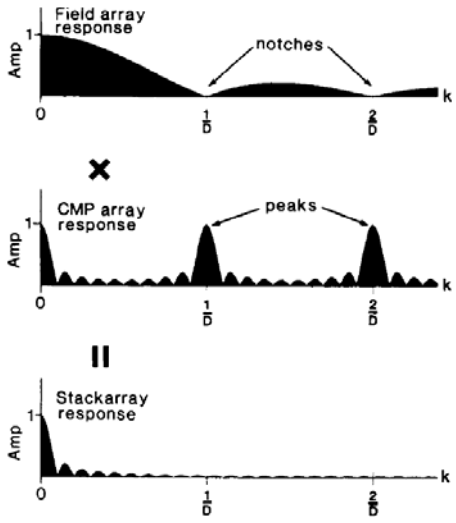

Figure 29
Stackarray wavenumber response.
Taken from (Morse et al, 1989)

The authors designed a 350-trace shot record consisting of a reflection event and ground roll to synthesize the individual shot records to be used with three field geometries. 30-trace end-on geometries A, B and C had arrays lengths of 30, 60 and 90 m respectively with an array-element spacing of 3 m, and shot and receiver intervals equal to 30 m.

For example, geometry B was synthesized by forming a 20-trace mix centered every 10th trace on the 350-trace record, which produced a reduced 30-trace shot record with a receiver interval of 30 m and an array length of 60 m. **Figure 30** depicts the stackarray responses of geometry A (discontinuous stackarray), geometry B (continuous uniformly weighted stackarray) and geometry C (continuous unevenly weighted stackarray). One can expect to obtain the best attenuation with Geometry B (60 m array).

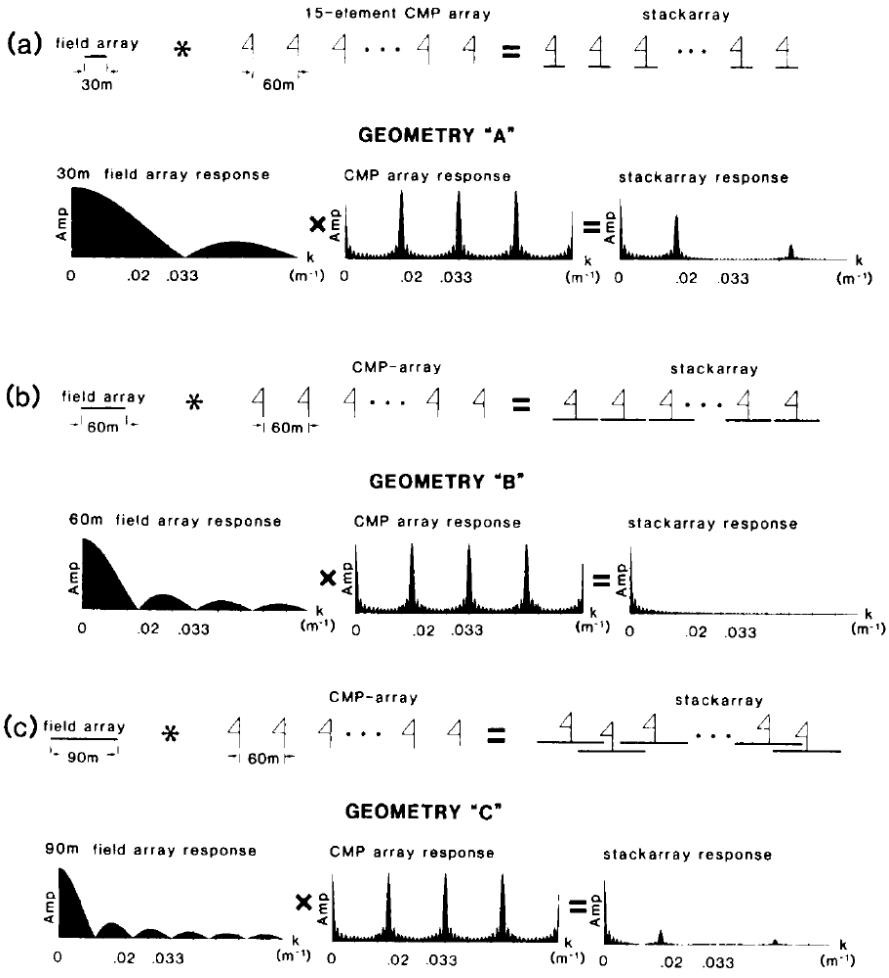

Figure 30
Stackarray responses of geometries A, B, and C.
Taken from (Morse et al, 1989)

Figure 31 shows the CMP gathers (top) and the CMP stacks after NMO (bottom). The signal-to-ground roll ratios for geometries A, B, and C before stack are 0.080, 0.2 and 0.308 respectively. Before stack, geometry C produced the highest S/G. The signal-to-ground roll ratios for geometries A, B, and C after stack are 0.626, 6.0 and 1.2 respectively. After stack, geometry B produced the best S/G. These results agree with the comment made in **Figure 30** that geometry B produced the best ground roll suppression.

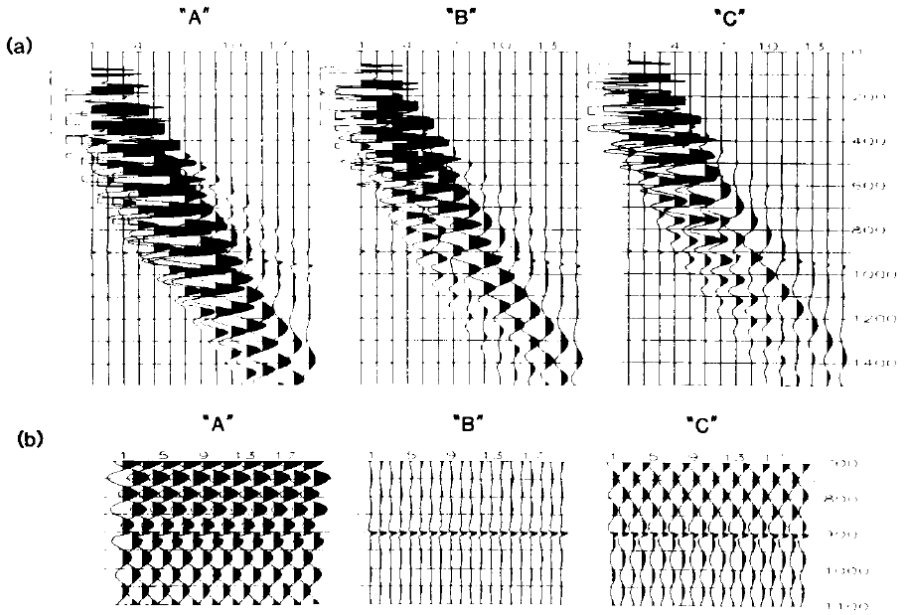

Figure 31
CMP gathers (top) and CMP stacks after NMO (bottom).
Taken from (Morse et al, 1989)

The authors concluded that the stackarray method is an effective technique to acquire 2-D seismic lines for ground roll suppression. Also, they recommend group spacings as small as possible in areas of severe ground roll.

This technique could be very expensive to acquire in areas that require heli-portable operations like in the foothills. It is more feasible for vibroseis operations than for dynamite. In vibroseis, one could shorten the source interval by two and decrease the number of sweeps by the same proportion at no extra acquisition cost, but in dynamite to double the number of holes is costly. The processing will be more expensive because the number of source points will double.

5. THE EFFECT OF GEOPHONE ARRAYS ON RANDOM NOISE (Levin, 1989)

There is a lot of talk about how arrays reduce coherent noise such as ground roll and air blast, but it they also attenuate other types of noise like random noise or scattered waves.

In this paper, the author studies the noise to signal ratio as a function of the ratio of geophone spacing to noise wavelength for linear arrays of 12, 24, 36 and 72 vertical and horizontal geophones. The noise-to-signal ratio is measured by $1/\sqrt{M}$, where M is the number of elements in the array.

Aki in 1957 and Denham in 1963 defined one type of random noise in which the value of the cross-correlation of the geophone responses was a Bessel function defined by $J_o(2\pi\Delta/\lambda)$, where Δ is the separation between geophones and λ the wavelength. Based on this function, the noise at one geophone is not independent of the noise at another geophone and their responses can be correlated.

Figure 32 compares the random noise/signal and the coherent noise/signal as a function of geophone spacing/noise wavelength (Δ/λ) for a linear array of 36 elements with equal sensitivities and equally spaced. In plot (a), for a given λ, the curve decreases rapidly and crosses the line $1/\sqrt{M}$ at a geophone spacing called the "coherent distance", and the curve increases when $\Delta=\lambda$, the recovery of N/S is less complete than for the coherent wave case. These experiments were repeated for different number of elements in the array, and the behaviors were similar, but the most effective reduction of random noise was obtained with the greatest number of geophones.

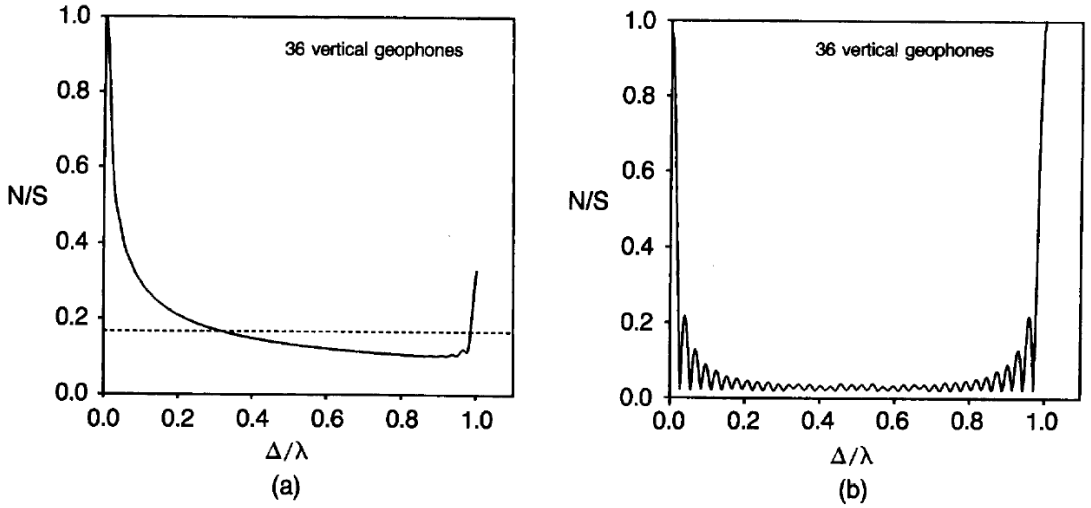

Figure 32
Random noise/signal versus coherent noise/signal responses.
Taken from (Levin, 1989)

Then the author proceeded to vary the separation and weight of the geophones in a similar fashion to the experiments conducted by Newman and Mahoney (Newman, 1973), and analyzed the N/S performance. He plotted the average of fifty curves in which the geophone weights were varied randomly with a 14 % standard deviation (**Figure 33**). The error introduced had almost no visible effect on the random N/S curve and coherent N/S curve. In the second case (**Figure 34**), the geophone separation was altered randomly; the average of the fifty curves shows a great impact on the array response and the random N/S curve shows a slightly lower reduction of noise below the $1 / \sqrt{M}$ line.

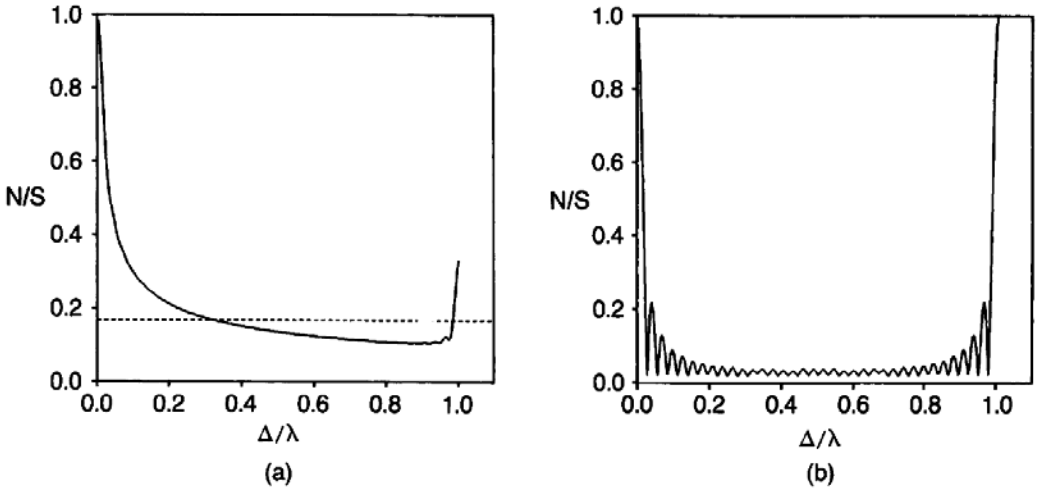

Figure 33
Average of 50 curves: random N/S (a) and coherent N/S (b) – error in weights-.
Taken from (Levin, 1989)

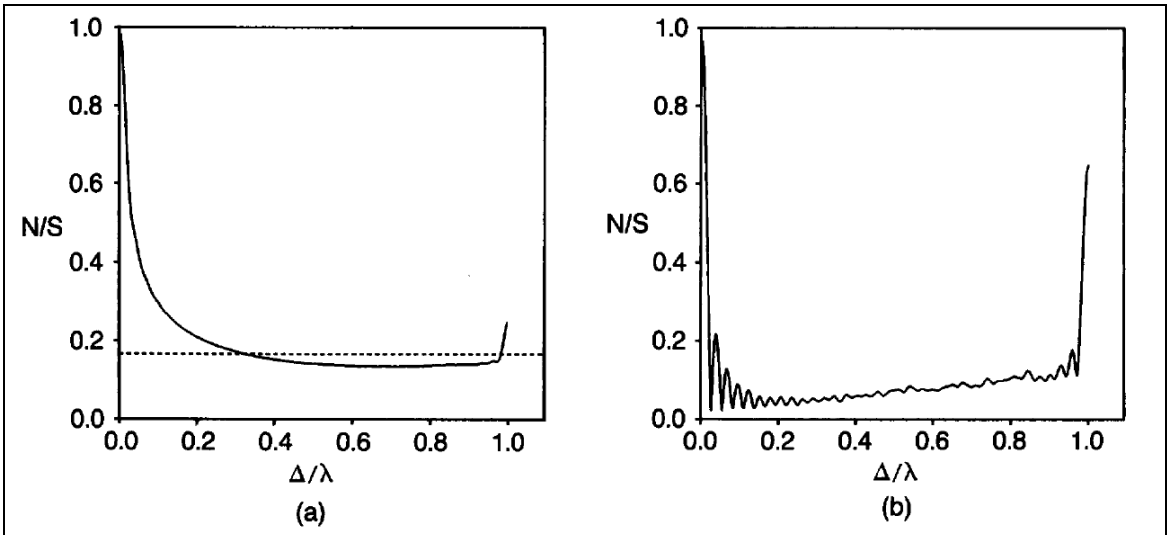

Figure 34
Average of 50 curves: random N/S (a) and coherent N/S (b) – error in positions-.
Taken from (Levin, 1989)

Figure 35 depicts the case in which both the geophone separation and the weights are randomly altered. The same observations made for the two previous figures can be made here, but they are more emphasized. **Figure 36** shows random N/S response as a function of Δ/λ for a 36-element array oriented along the spine of the array when the noise has a SV type motion, plot (a), and SH type motion, plot (b). One can observe that the noise level decreases greatly with the SV type motion.

This paper is only valid for random noise types described by a Bessel function. When comparing these results to the ones obtained by Newman and Mahoney, one should have in mind that the N/S scale is not a logarithmic scale. This linear scale makes the array responses look different from the results obtained by Newman and Mahoney, when in reality they are similar.

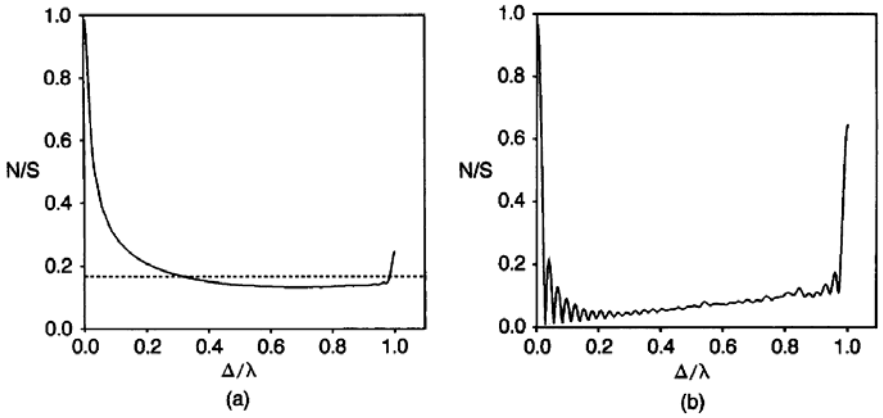

Figure 35
Average of 50 curves: random N/S (a) and coherent N/S (b) – error in posit. and weights-.
Taken from (Levin, 1989)

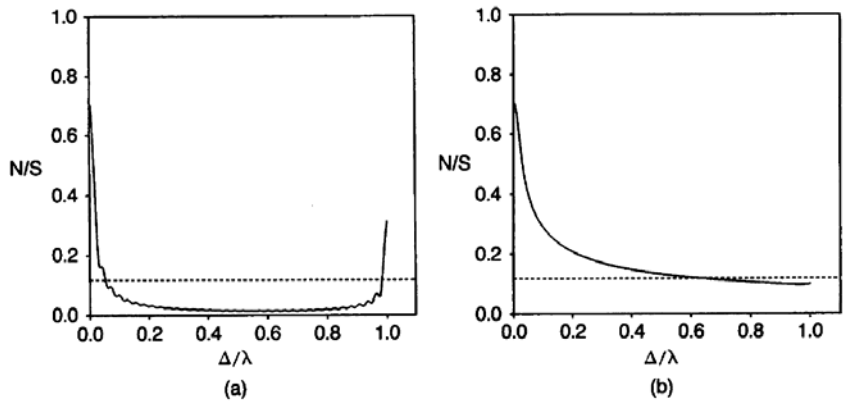

Figure 36
SV type (a) and SH (b) type noise motion.
Taken from (Levin, 1989)

6. SYSTEM DESIGN FOR BETTER SEISMIC DATA (Pritchett, 1991)

In this paper Pritchett sets array design guidelines for better seismic data. He states that it is imperative to suppress very strong noise in the field, but not at the expense of the signal. His guidelines specify that:

- The data has to be recorded in a manner consistent with stack array and that the receiver interval chosen will not alias the high frequency components of the reflections from zones of interest.
- Use long linear receiver arrays with at least 12 elements separated in such a way that will suppress the short wavelengths of the airwave.
- Complement your receiver array with a source array.

The most important conclusion from his paper is that the source array is to produce suppression notches where the geophone array has leak side lobes.

A source pattern works two ways: it suppresses ambient noise by effectively directing source energy so as to increase the reflection amplitudes, and it suppresses source-generated noise with the normal array response. In order to obtain better results, we add together the geophone array response with the source array response. If we use vibrators as a source of energy, the drag response can also be added.

7. 3-D SYMMETRIC SAMPLING IN THEORY AND PRACTICE (Vermeer, 1998)

This paper deals with all the aspects required to achieve symmetric sampling:

- Shot station equal to the receiver station.
- Shot line spacing equal to the receiver line spacing.
- Maximum offset inline equal to the maximum offset crossline.
- Shot arrays required as much as receiver arrays.

Linear arrays are sufficient for alias protection in the cross-spread. The receiver arrays look after the noise in the source gathers and the source arrays attenuate the noise in the receiver gathers. Each array takes care

of one (in-line or cross-line) component of noise. He recommends to sample the signal without aliasing and to use arrays to take care of the ground roll.

8. INSTRUMENTATION OR HOW MANY SOWS' EARS DOES IT TAKE TO MAKE A SILK PULSE? (Cambois, 2002)

In this paper Cambois talks about types of geophones, digital sensors, dynamic range and recording systems and how they have evolved throughout the years. He comments on the Q System introduced by Schlumberger in 2000, having more than 30,000 geophones available. This system records every trace as a point receiver and then they form offset variant arrays based on the knowledge that far offsets have shorter apparent wavelength and near offsets have longer apparent wavelengths because they experience less moveout.

Cambois mentions that the digital array forming can achieve greater noise reduction that the analog arrays, being a further development on the square root law. The challenge with this system is the huge amount of equipment that has to be deployed simultaneously. **Figure 37** depicts the square root law in which the signal increases in proportion to the number of times it is recorded, while Gaussian distributed random noise increases only in proportion to the square root.

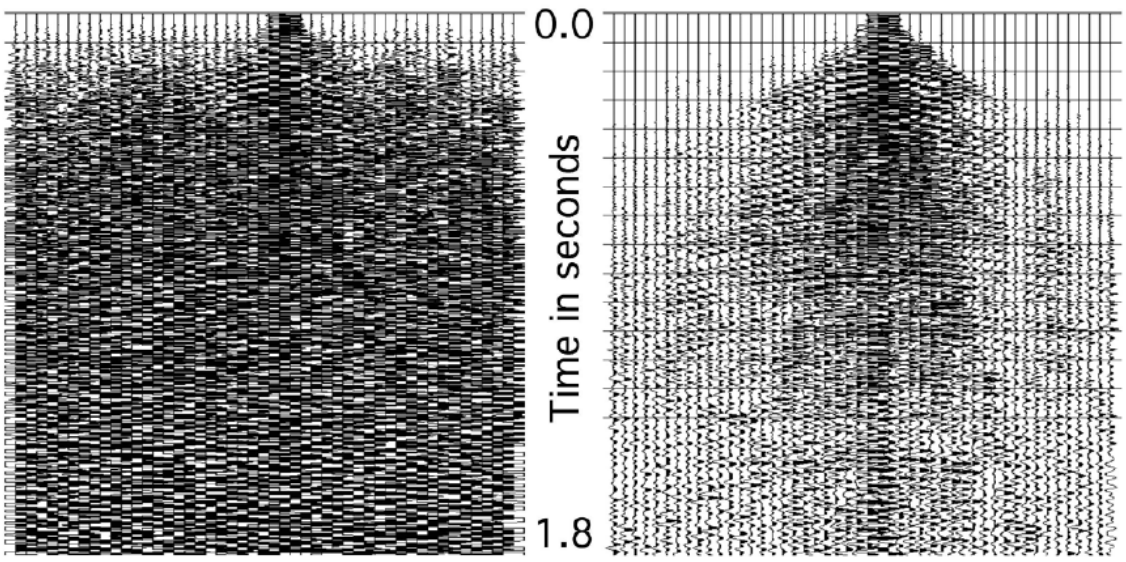

Figure 37
One single sweep (left) versus same sweep repeated 1280 times (right).
Taken from (Cambois, 2002)

9. KEY ELEMETS OF TOTAL SEISMIC FIELD DESIGN USING MATHEMATICA – A TUTORIAL (Benyamin, 2002)

Benyamin starts his introduction by citing Steve Roche's question (Roche, 2001) of point sources and point receivers ever overcoming the current benefits of signal-to-noise ratios provided by arrays.

One school of thought promotes the use of point sources and point receivers stating that with seismic data processing an optimal bandwidth and signal-to-noise ratio can be achieved, and therefore, there is no need for arrays. The problem with this thought is that in that wavenumber range in which signal and noise are mixed and cannot be separated, by using several geophones per group we not only remove some coherent and incoherent noise, but also statistically improve the average output by means of the superposition principle and geophone coupling, and also provide an anti-alias filter; therefore arrays are beneficial.

In this paper the author explains the equations that represent the array response in the time and frequency domain. Mathematically, a normalize response (with respect to the sum of the element weights) of the array in the time domain is:

$$h(t) = \frac{1}{\sum_{n=1}^{m} a_n} \sum_{n=1}^{m} a_n \delta(t - t_n) \qquad (4)$$

The Fourier transform of this response in the frequency domain is:

$$H(\omega) = \frac{1}{\sum_{n=1}^{m} a_n} \sum_{n=1}^{m} a_n e^{-j\omega t_n} \qquad (5)$$

where t_n represents the delay of the nth element with respect to the reference and $\omega = 2\pi f$. To represent equation (5) in the wavenumber domain, having n elements separated by a distance d and using as a reference the first element, then $t_n=(n-1)d/v = (n-1)d/f\lambda = k(n-1)d/f$, where k and λ are apparent wavenumber and wavelength respectively. Replacing t_n in equation (5) we get:

$$H(k) = \frac{1}{\sum_{n=1}^{m} a_n} \sum_{n=1}^{m} a_n e^{-j2\pi k(n-1)d} \qquad (6)$$

If all the elements of the linear array have the same weight, then $a_n = 1$. In the case of areal arrays, one has to project the elements of the

array onto a given direction, having then a linear array with variable weights (in this case a_n will be equal to the different weights).

This paper is interesting from the mathematical representation of the arrays and for the initial discussion of point sources and point receivers versus the benefits of arrays.

10. IMPROVING SEISMIC DATA QUALITY WITH HIGH-DENSITY DATA ACQUISITION (May, 1986)

In this paper the author compared two 2-D seismic lines acquired simultaneously. One line had a receiver interval of 240 ft and a receiver array length of 235 ft. The second line had a group interval of 60 ft and a receiver array length of 55 ft. The second receiver line is called "high-density seismic acquisition" because it reduces the group interval and increases the sampling of the wave field. The term "high-density data" is being used frequently these days in seismic acquisition and this paper was chosen for that reason.

The high-density data were processed intact and computer-summed to simulate the long array data. Both the intact and the computer summed stacks show better S/N and lateral and temporal resolution than the data acquired with the long arrays (see **Figure 38**).

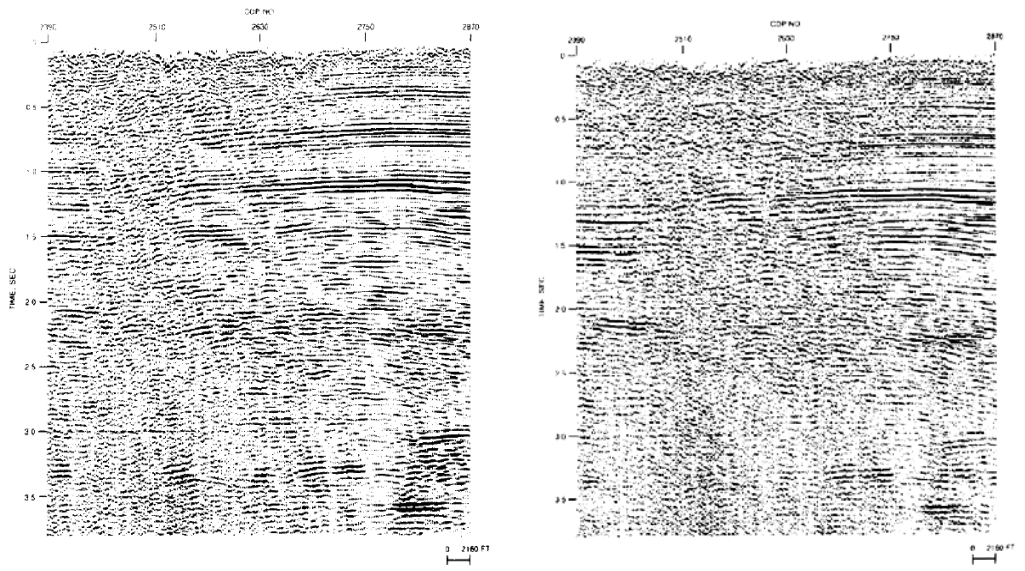

Figure 38
Computer–summed (left) and conventional (right) CDP stacks.
Taken from (May, 1986)

With a receiver array length of 55 ft, the first notch of the array response should be placed at a k=0.018 ft^{-1}. An array length of 235 ft will produce the first notch at k=0.0042 ft^{-1}. As shown in the background review, the longest wavelengths of signal we can expect for a deep reflector are approximately 262 ft long (80 m) with a wavenumber of 0.0038 ft^{-1}. Just by looking at the wavenumbers, one can see that the long array will be attenuating the signal compared to the short array. With a receiver interval of 240 ft, the longest wavelengths are being sampled only once, contrary to the Nyquist theory. These are the reasons why the high-density data looks better.

11. ON THE RESPONSE OF HYDROPHONES AND GEOPHONES IN A TRANSITION ZONE ENVIRONMENT (Moldoveanu et al, 1995)

In the past, people had obtained mixed results using geophone arrays in transition zone environments (Moore et al, 1993). Since 1993 there have been a group of people using hydrophones instead of geophones in transition zones, claiming that the buried hydrophone technique produced better data quality. This presentation is an example of people promoting the use of single detectors instead of geophone arrays.

The near surface conditions of the survey were about 10 ft of water followed by 100 ft of muddy sediments. In their experiment, they buried at each receiver location two hydrophone-geophone pairs at a depth of 1 and 25 ft below the water bottom. The 2-D line had 85 receiver stations with an interval of 220 ft, 138 shot points, offsets up to 17,000 ft and maximum fold of 62. The same processing sequence was applied to both cases.

Figure 39 and **Figure 40** show that better S/N is achieved with the hydrophones than with the geophones. The reflectors are not only stronger, but they also have more continuity. The authors believe that the reason for the S/N improvement is due to the near perfect ground coupling of hydrophones in water saturated muddy sediments.

The authors concluded that hydrophones generated better quality stack sections in this area of southern Louisiana, and that the quality also improved with depth of burial. It would have been interesting to compare the hydrophone/geophone stack sections with a section generated with geophone arrays.

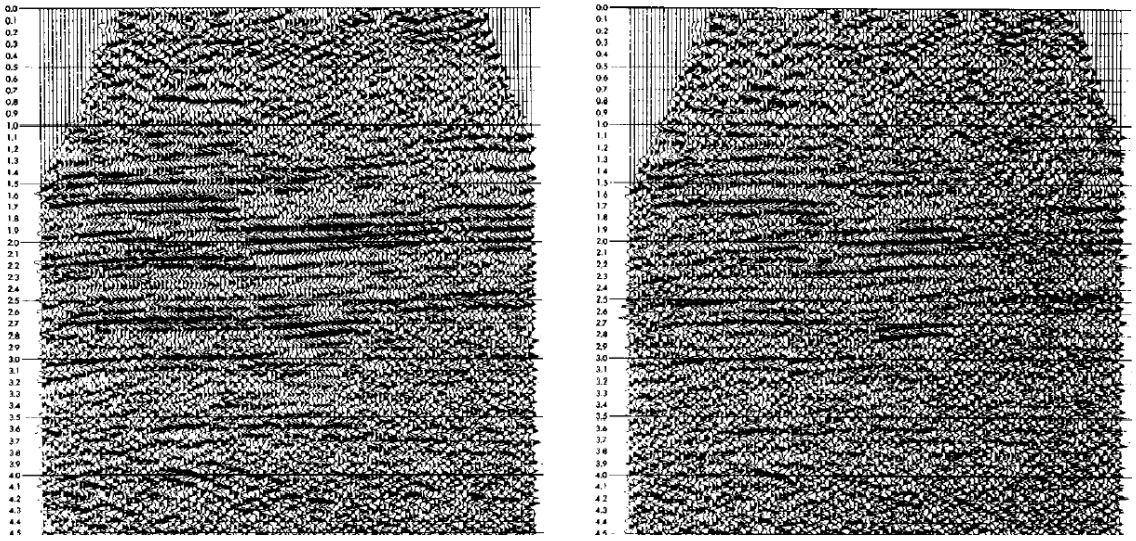

Figure 39
Stack section produced with hydrophones (left) and geophones (right) buried at 1ft.
Taken from (Belcher, 1986)

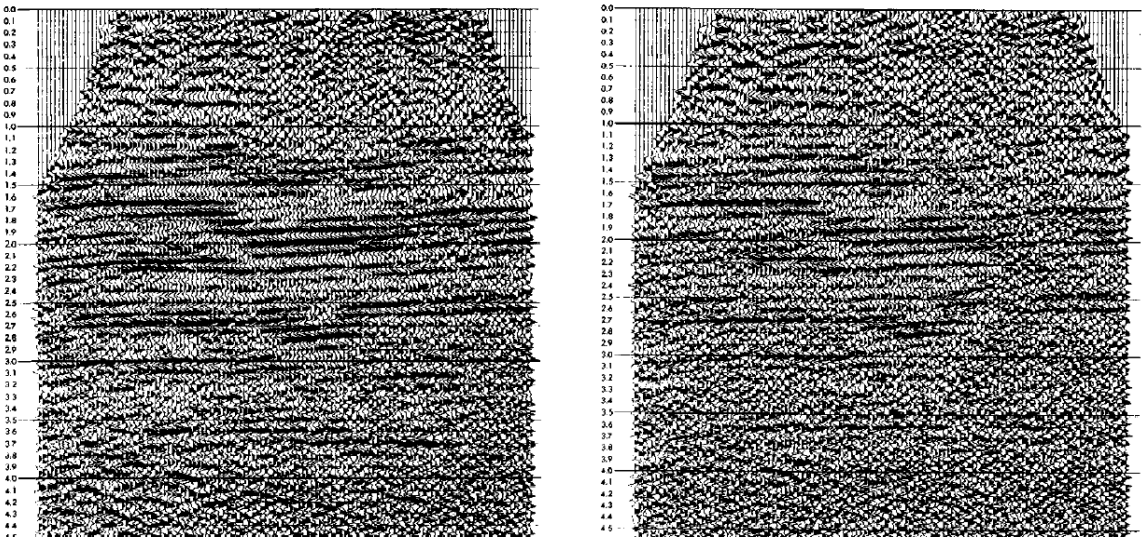

Figure 40
Stack section produced with hydrophones (left) and geophones (right) buried at 25 ft.
Taken from (Belcher, 1986)

12. ALTERNATIVE PROCESSING TECHNIQUES AND DATA IMPROVEMENT PROVIDED BY SINGLE-SWEEP RECORDING (Belcher et al, 1986)

This paper promotes an alternate method of recording vibroseis data in which each pad position within the source array becomes a source point. The authors state that by processing each sweep as a separate point, increased lateral resolution can be achieved.

From the 2-D field parameters given in the paper, one can deduce that the source interval was equal to the receiver interval and equal to 69 m. The effective length of the source array was also equal to 69 m. One vibrator was used shaking 16 sweeps (recorded individually) spaced 4.5 m apart.

The conventional method of acquiring vibroseis data at that time, consisted of summing all the pad positions within a source array, apply the correlation and then AGC the data to produce a shot record. The alternate method proposed consists of applying an AGC to the individual records, then apply the vibroseis correlation and finally, sum them together. To apply AGC before the correlation is a form of whitening the spectrum of the data. They promote this method if the geophysicist is not interested in true amplitude recovery.

Figure 41 shows two shot records with AGC (spectral whitening) applied before and after summing the individual records. The authors claim improved S/N and resolution in the shot record that had the spectral whitening applied to the individual records before summing.

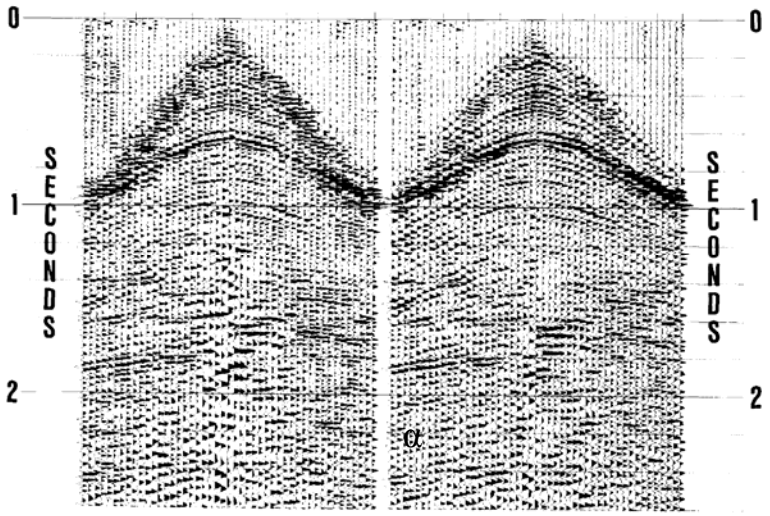

Figure 41
AGC applied after summing (left) and before summing individual records (right).
Taken from (Belcher, 1986)

Based on ray theory, the reflection points from a common receiver and each one of the vibrator pad locations in the source array are distributed in the subsurface along a segment of a reflector that is equal to half the array length. The signal is averaged over the length of that segment. The authors say that each reflection is made of contributions from Fresnel zones and that the area of largest contribution is centered around the common reflection point. The Fresnel zones overlap between each reflection point, but when the records are summed together, they are averaged over an area smaller than the corresponding records summed in a source array. This smaller area is due to the whitening of the spectrum that shrinks the Fresnel zone.

If this is the case, the improvement in lateral resolution is achieved not by applying an AGC to the individual records before the correlation and summing, but by the smaller sampling. This also indicates that the receiver and source intervals chosen for this 2-D line are not adequate.

13. THE EFFECTS OF SPATIAL SAMPLING ON REFRACTION STATICS (Palmer et al, 2000)

In this paper, Palmer et al study the effects of geophone arrays on the inversion process. They used two coincident sets of data recorded in Southeastern Australia. One set of data used a receiver interval equal to 60 m with the 16 receivers in the array placed end-to-end, and the other set used point receivers 10 m apart.

Unfortunately, in the conference abstract there are no images to support the conclusions. The authors concluded that the vertical resolution achieved with the 60 m arrays was poor (not measuring the thickness of the weathering layer correctly), as opposed to the results obtained with the point receivers. They claimed that the length of the 60 m array was the significant factor limiting the resolution of the refraction data.

Based on this poor information provided, let us build the array attenuation curve for the 2 cases: point receiver and 16-element array (see **Figure 42**). The black vertical line at 0.022 m-1 depicts the signal wavenumber range. If the zone of interest was a shallow one, the signal wavenumber range would be between 0 and 0.025 and the 60 m array would be too long as observed in the graph. There would be too much signal attenuation; notice that the black line is past the first notch. If the zone of interest is a deep reflector, then our signal range would be to the left of the first notch, but when compared to the 10 m point receiver zero attenuation (blue horizontal line) it would weaker. This reasoning leads me to conclude that the array used for this experiment was too long, as well as the group interval.

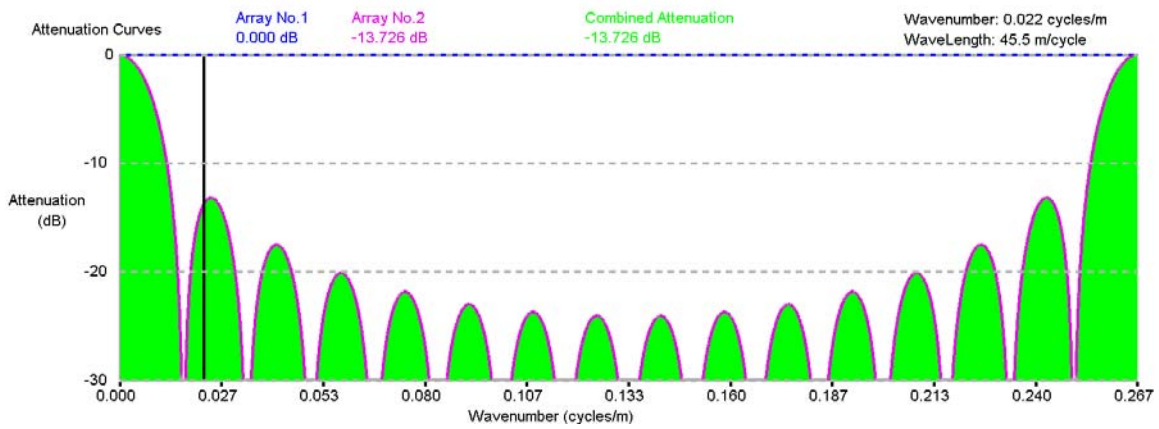

Figure 42
16-element array over 60 m versus point receivers every 10 m.

14. CASE HISTORY

In the field, geophone and source arrays interact to suppress undesired noise. In order to optimize array systems the following guidelines are recommended (Norm Cooper, 2000): first, the effective length of the longest sub-array should be equal to the longest wavelength desired in the reject band. Make sure that all seismic signal lies within the first lobe. Second, for a two sub-array system, the effective length of the second sub-array should be about 70 % of the first one. Finally, for a three sub-array system, the effective length of the second sub-array should be about 80 % of the first one, and the effective length of the third sub-array should be about 80 % of the second one.

In this field example, a three sub-array system was analyzed. The objective was to determine during testing if the drag array was going to be beneficial compared to the center stack. The geophone array was formed by 6 geophones spread over 20 meters having its first maximum attenuation at 0.05 m^{-1}, see **Figure 43**. The second array is the vibrator disposition array: 2 vibrators over 30 meters (15 m pad to pad) and its reject zone starts at 0.033 m^{-1}, see **Figure 44**. The third array is the drag array: 2 sweeps over 20 meters (10 m between successive pad positions) with its maximum attenuation happening at 0.05 m^{-1}, see **Figure 45**.

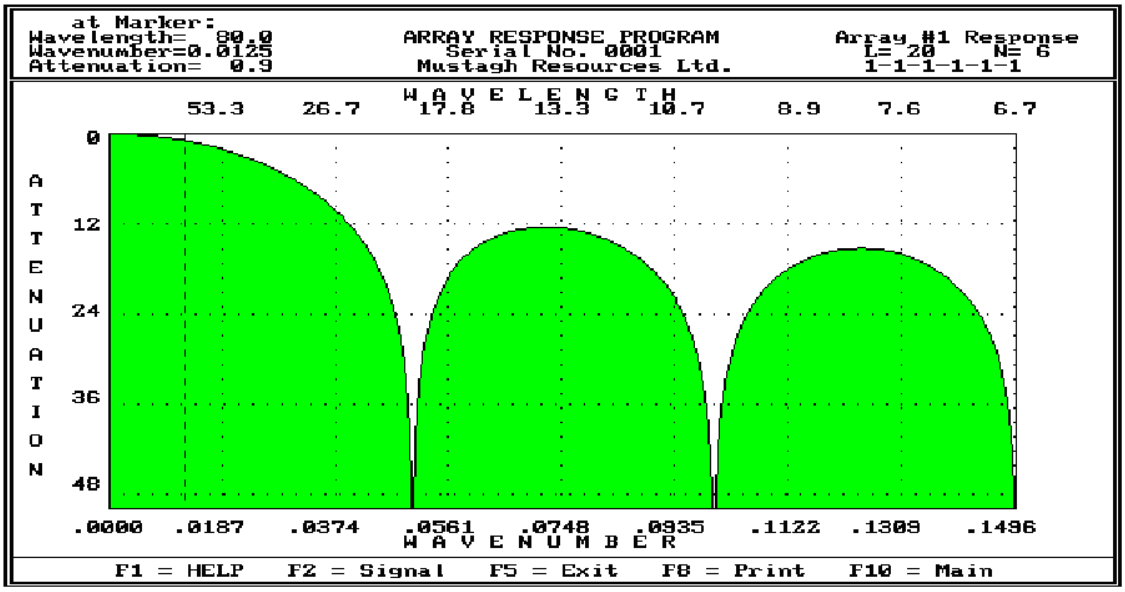

Figure 43
Geophone array – 6 over 20 meters.

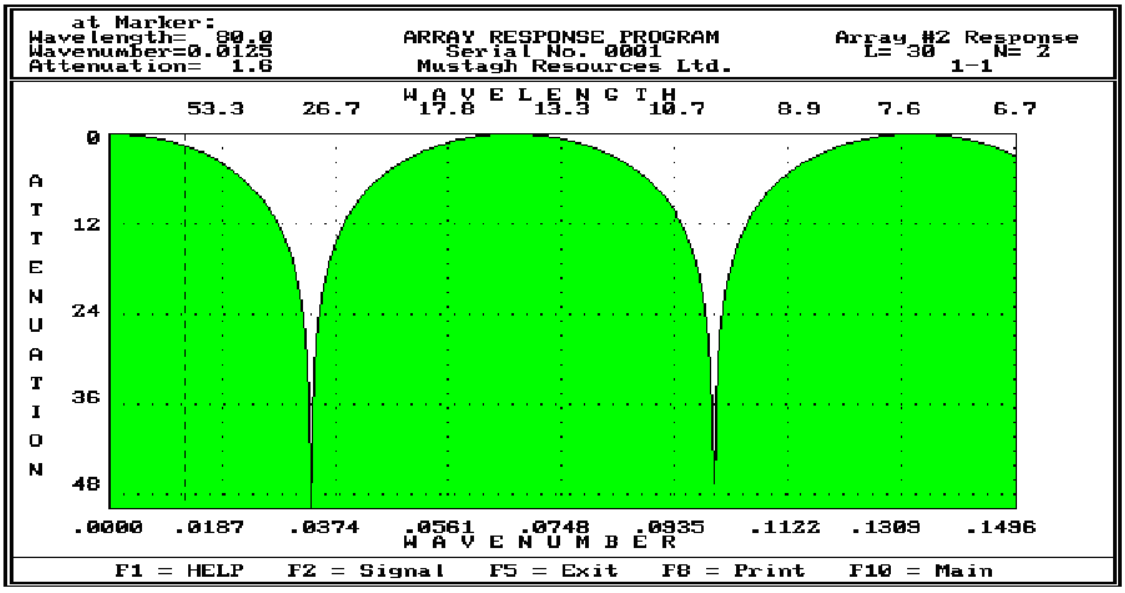

Figure 44
Vib disposition array- 2 over 30 meters (15 m pad to pad).

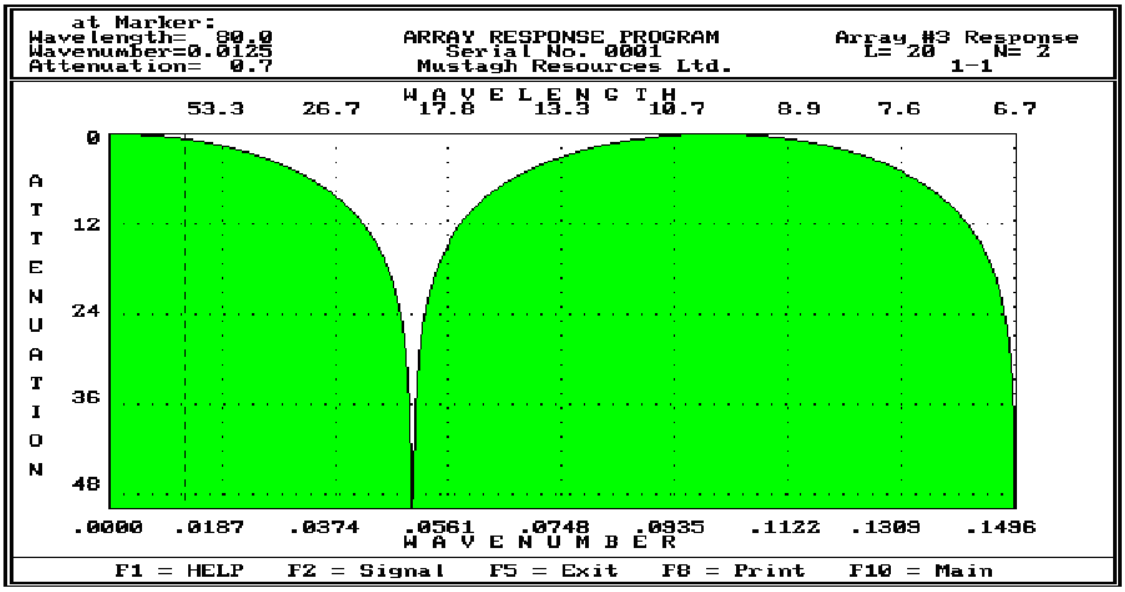

Figure 45
Drag array – 2 sweeps over 20 meters (10 m move-up).

The next two figures show the combined array response. **Figure 46** shows the response of the three arrays: geophone, vib disposition and drag. **Figure 47** shows the sum of all arrays without the drag. In theory, the drag combined with the other arrays should yield a better noise attenuation. Around 30 dB are attenuated with the drag and about 20 dB are attenuated without the drag.

Based on the results from Newman and Mahoney (1973), an array implementation error between 10 and 20 % reduces the maximum attenuation of the reject band to 24 dB. This means that in the field, with the implementation errors, it is not realistic to expect attenuation greater than 24 dB. Therefore, even though the drag array provides better results in theory, the stacked sweep was chosen.

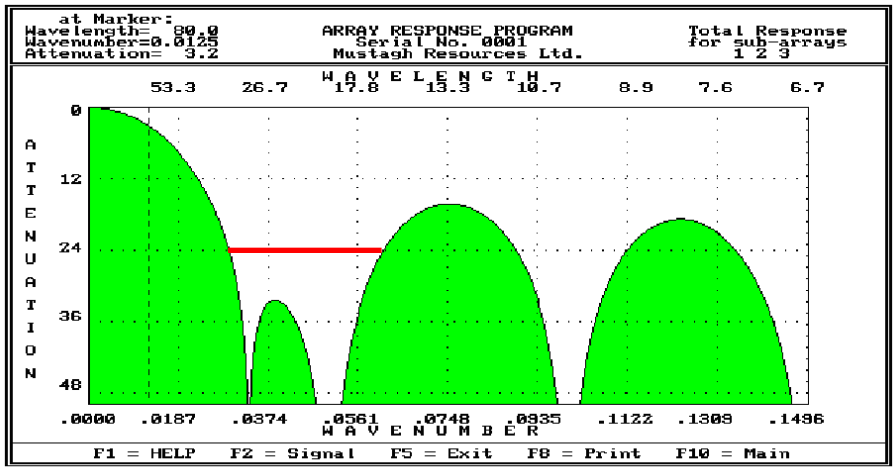

Figure 46
Combined array response.

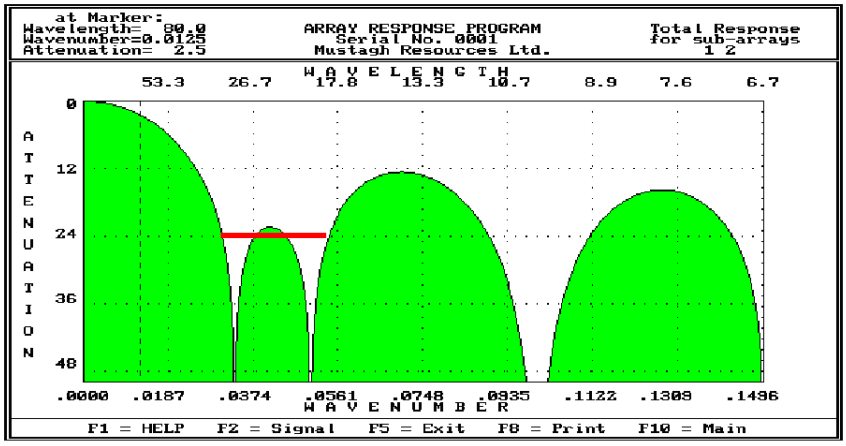

Figure 47
Sum of all arrays without drag.

Bibliography

1. Aki, K., 1957. Space and time spectra of stationary stochastic waves, with special reference to microtremors: Bulletin of Earthquakes Res. Inst., Vol. 35: 415 - 456.

2. Anstey, Nigel A. 1986. Whatever happened to ground roll?: Geophysics: The Leading Edge of Exploration, March: 40 – 45.

3. Belcher, Steven, Pratt, Thomas, Costain, Jhon and Coruh, Cahit. 1986.Alternative processing techniques and data improvement provided by single-sweep recording: Geophysics, Vol. 51, No. 9:1736-1742.

4. Benyamin, Ninos. 2002. Key elements of total seismic field design using mathematica – A tutorial: Geophysics, Vol. 67, No. 4:1020-1027.

5. Cambois, Guillaume. 2002. Instrumentation or how many sows' ears does it take to make a silk purse?: The Leading Edge, September: 816-818.

6. Cooper, Norman. 2000. Land seismic acquisition course notes.

7. Cooper, Norman. Personal communication on March 12, 2005.

8. Denham, D. 1963. The use of geophone groups to improve the signal-to-noise ratio of the first arrival in refraction shooting: Geophysical Prospecting, Vol. 11: 389 – 408.

9. Evans, Brian. 1997. A Handbook for Seismic Data Acquisition in Exploration: Geophysical Monograph Series, Number 7, SEG.

10. Hoffe, Brian H., Margrave, Gary F., Stewart, Robert R., Foltinek, Darren S., Bland, Henry C. and Manning Peter. 2002. Analizing the effectiveness of receiver arrays for multicomponent seismic exploration. Geophysics, Vol. 67, No. 6: 1853-1868.

11. Levin, Franklyn K. 1989. The effect of geophone arrays on random noise: Geophysics, Vol. 54, No. 11: 1146 – 1473.

12. May, T. W. 1986. Improving seismic data quality with high-density data acquisition: Geophysics, Vol. 51, No. 8:1700-1701.

13. Moldoveanu, N., Spradley, M., Lang, J., Brooks, T. and Chand, M. 1995. On the response of hydrophones and geophones in a transition zone environment: SEG Technical Meeting Abstracts 65, 999-1002.

14. Moore, D., Luzietti, G., Moldoveanu, N., Spradley, M., Brooks, T. and Chang, M. 1993. Innovation and flexibility: The keys to a successful 3-D survey in the transition zone area of West Bay Field, Southern Louisiana: SEG Technical Meeting Abstracts 63: 999-1000.

15. Morse, Peter F. and Hildebrandt, George F. 1989. Ground-roll suppression by the stack array: Geophysics, Vol. 54, No. 3: 290 – 301.

16. Newman, P. and Mahoney, J. T. 1973. Patterns – with a pinch of salt: Geophysical Prospecting, Vol. 21: 197-219.

17. Palmer, Derecke, Goleby, Bruce and Drummond, Barry. 2000. The effects of spatial sampling on refraction statics: Exploration Geophysics, Vol. 31, No 1 & 2: 270 – 274.

18. Pritchett, William. 1991. System design for better seismic data: Geophysics: The Leading Edge of Exploration, November: 30 - 35.

19. Rigdon, H. K. and Thomas, J. W. 1987. Evaluation of seismic arrays in the temporal frequency domain: Geophysics: The Leading Edge of Exploration, November 1987: 40-46.

20. Roche, Steve. 2001. Seismic data acquisition-The new Millennium: Geophysics, Vol. 66, No. 1:54.

21. Vermeer, Gijs. 1998. 3-D symmetric sampling: Geophysics, Vol. 63, No. 5: 1629 – 1647.

22. Vermeer, Gijs. 1998. 3-D symmetric sampling in theory and practice: The Leading Edge, November: 1514 – 1519.

23. Vermeer, Gijs J. O. 1999. Factors affecting spatial resolution: Geophysics, Vol. 64, No. 3: 942 - 953.

24. Vermeer, Gijs J. O. 2003. Discussion on analyzing the effectiveness of receiver arrays for multicomponent seismic exploration: Geophysics, Vol. 68, No. 5: 1760.